Since January 2020 Elsevier has created a COVID-19 resource centre with free information in English and Mandarin on the novel coronavirus COVID-19. The COVID-19 resource centre is hosted on Elsevier Connect, the company's public news and information website.

Elsevier hereby grants permission to make all its COVID-19-related research that is available on the COVID-19 resource centre - including this research content - immediately available in PubMed Central and other publicly funded repositories, such as the WHO COVID database with rights for unrestricted research re-use and analyses in any form or by any means with acknowledgement of the original source. These permissions are granted for free by Elsevier for as long as the COVID-19 resource centre remains active.

Journal of Molecular Graphics and Modelling 109 (2021) 108038

Contents lists available at ScienceDirect

Journal of Molecular Graphics and Modelling

journal homepage: www.elsevier.com/locate/jmgm

In silico identification of SARS-CoV-2 cell entry inhibitors from selected natural antivirals

Yusuf Şimşek [a,*], Sahra Setenay Baran [b], Belma Aslım [b]

[a] *Vocational School of Health Services, Gazi University, Ankara, Turkey*
[b] *Department of Biology, Gazi University, Ankara, Turkey*

ARTICLE INFO

Keywords:
SARS-CoV-2
Antivirals
Spike protein
Neuropilin
ACE2
Molecular docking
Molecular dynamics simulation

ABSTRACT

The aim of this study is to identify potential drug-like molecules against SARS-CoV-2 virus among the natural antiviral compounds published in the Encyclopedia of Traditional Chinese Medicine. To test inhibition capability of these compounds first, we docked them with Spike protein, angiotensin-converting enzyme 2 (ACE2) (PDB ID: 6M0J) and neuropilin 1 (NRP1) (PDB ID: 7JJC) receptors, and found significant docking scores with extra precision up to −11 kcal/mol. Then, their stability in the binding pockets were further evaluated with molecular dynamics simulation. Eight natural antiviral compounds were identified as potential inhibitors against SARS-CoV-2 cell entry after 200 ns molecular dynamics simulations. We found CMP-3, CMP-4, CMP-5, CMP-6 and CMP-8 are strong binders for the spike protein, CMP-1, CMP-2, CMP-4, CMP-5 and CMP-7 are strong binders for the neuropilin receptor, and CMP-5 is a strong binder for the ACE2. Quercetin derivatives (CMP-4, CMP-5, CMP-6 and CMP-7) were found highly stable in the active domain of NRP1, ACE2 and Spike protein. Especially, CMP-5 showed an inhibitory activity for all targets. These natural antivirals may be potential drug candidates for the prevention of SARS-CoV-2 infection.

1. Introduction

Around December 2019 in Wuhan city, Hubei province of China, a severe and highly contagious viral disease that causes concentrated pneumonia cases were reported by the Wuhan Municipal Health Commission [1]. As of September 2021, nearly 222.5 million people have been affected and 4.6 million people lost their life all over the world [2]. The outbreak was attributed to a novel coronavirus (SARS-CoV-2) that has genetic similarities with previously known coronaviruses (Bat-SL-CoVZXC2 and bat-SL-CoVZC45) [3], and the disease was named as coronavirus disease 2019 (COVID-2019) by the WHO. As of April 2021, there is no proved antiviral drugs specific for COVID-19, but various approved antiviral drugs have been used and studied since outbreak emerged. Lopinavir developed as a human immunodeficiency virus 1 (HIV-1) protease inhibitor has been used safely in combination with ritonavir [4] with limited side effects and a good efficacy [5]. Additionally, lopinavir/ritonavir has been reported to have antiviral activity against SARS-CoV [6] and MERS-CoV [7]. Therefore, it was considered as an option for treating SARS-CoV-2 [8–11]. Although the lopinavir/ritonavir did not show significant benefits for severe COVID-19 patients [12–15], it was advised as a supportive care for mild COVID-19 patients [16]. Ribavirin, which was used for SARS-CoV [17,18] and MERS-CoV [19–21] and associated with serious side effects [19,22], has been recommended at the beginning of the outbreak in China, but its efficacy remained controversial, even though it showed some beneficial effects in the treatment of COVID-19 patients [20,23]. Favipiravir, which was originally designed for influenza with inhibiting the RNA polymerase of RNA viruses, showed an antiviral activity against SARS-CoV-2 [24–27] at high doses and reduced healing time [28,29]. Remdesivir is one of the most promising antiviral drugs against a wide variety of RNA viruses [30–32], and the Food and Drug Administration issued permits the use remdesivir in the treatment of patients infected with SARS-CoV-2. In a double-blind, randomized, placebo-controlled study, patients who used remdesivir had a shorter recovery time and lower respiratory tract infection than the patients in the placebo group did [33,34]. Although remdesivir inhibits SARS-CoV-2 in human lung cells [35], a serious side effects have been reported and the treatment was halted [36] because further explorations were needed to verify its benefits and safety [37–39]. Hydroxychloroquine and chloroquine were first developed against malaria. Besides the treatment of malaria disease, they have been used for the treatment of various rheumatic diseases [40]. When COVID-19 outbreak spread all over the world,

* Corresponding author.
E-mail address: yusufsimsek@gazi.edu.tr (Y. Şimşek).

https://doi.org/10.1016/j.jmgm.2021.108038
Received 15 July 2021; Received in revised form 15 September 2021; Accepted 22 September 2021
Available online 29 September 2021
1093-3263/© 2021 Elsevier Inc. All rights reserved.

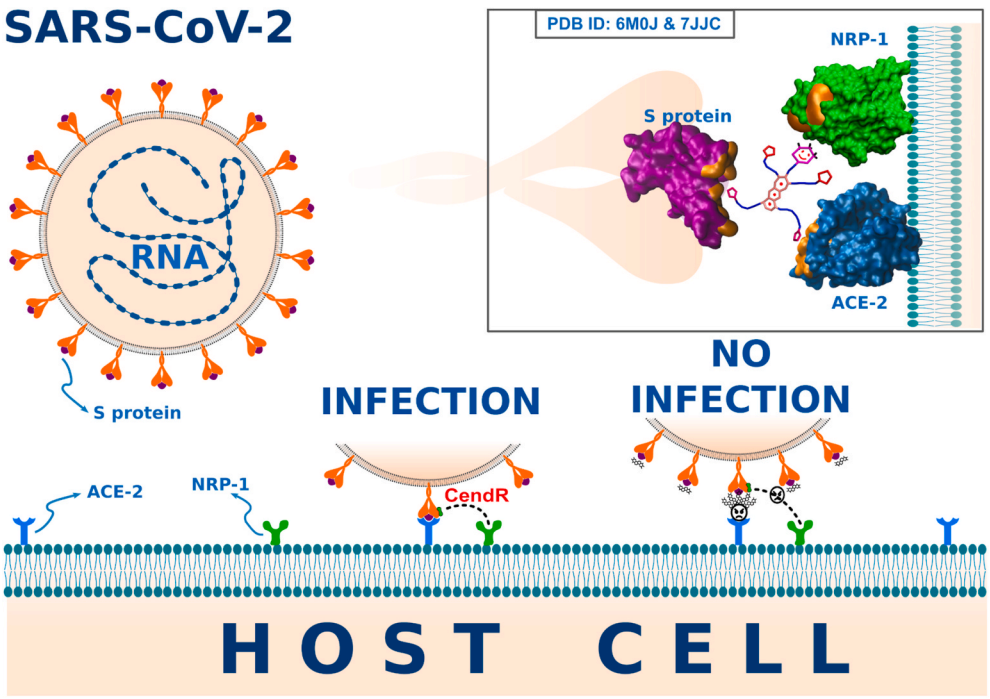

Fig. 1. Mechanism of action to prevent SARS-CoV-2 entry into human cell. Viral transmission of the SARS-CoV-2 starts after the interaction of the S protein with the host ACE2 and NRP1 receptors. Preventing protein-protein interactions between S protein and receptors via inhibiting receptor binding domains of S protein, peptidase domain of the ACE2 and b1 ectodomain of NRP1 receptors with antiviral compounds is an important approach for developing therapeutics against SARS-CoV-2.

hydroxychloroquine and chloroquine were attracted by the researchers because of their antiviral properties and considerable benefits have been reported in the patients infected with SARS-CoV-2 especially when these drugs were combined with Azithromycin [41–43]. However, the dose used for SARS-CoV-2 treatments is much higher than the recommended optimal dose (400 mg/day) for malaria treatments [44]. Additionally, some side effects, such as prolongation in the QT interval due to blocks the KCNH2 encoded hERG/Kv11.1 potassium channel [45] and retinopathy, were reported [46–49].

Despite the above preliminary antiviral evidences of drugs originally developed for HIV, SARS-CoV and MERS-CoV against SARS-CoV-2, the development of efficient and proven drugs specific to SARS-CoV-2 is still urgent. In this context, several major targets, such as non-structural protein complex, main protease, papain-like protease and RNA-dependent RNA polymerase, have been considered for drug discovery [50,51]. Generally, these are the important targets to prevent the replication and translation process of the virus in host. Another important approach is to suppress the viral binding between the virus proteins and the proteins of the host cell [52]. Viral transmission of the SARS-CoV-2 starts after the interaction of the spike (S) protein, a type I glycoprotein on the surface of the virus, with the host angiotensin-converting enzyme 2 (ACE2) receptor. Once the S protein makes viral binding to the ACE2 protein, fusion to the host cell membrane starts after the cleavage of the S protein by the host transmembrane protease serine 2 (TMPRSS2) [53–55]. Therefore, preventing protein-protein interactions (see Fig. 1) between S protein and ACE2 receptor via inhibiting receptor binding domain (RBD) of S protein and peptidase area of the ACE2 receptor with drug molecules is an important approach for developing therapeutics against SARS-CoV-2 [55].

Additional to ACE2 receptor, a recent experimental study [56] showed that neuropilin (NRP) receptor, which regulates axon guidance, angiogenesis and vascular permeability, can play an important role in the rapid infection of SARS-CoV-2. The cleavage of the poly-basic domain of S protein by furin motivates the formation of C-end Rule (CendR) motif in the C-terminal of S protein, which corresponds to 682–685 residue numbers. It is also reported that the infectivity of SARS-CoV-2 increased when CendR motif interacts with the b1 ectodomain of NRP1, and these viral interactions could be reason of severe neuronal symptoms seen in COVID-19 patients. Hence, blocking of b1 ectodomain of NRP1 is another important strategy for developing therapeutics against SARS-CoV-2 [56,57].

Since the COVID-19 outbreak, a variety of inhibitors have been found through screening and structure based design approaches among small molecules, natural compounds and approved drugs taken from the SWEETLEAND library [58], Swiss Target Prediction website [59], LOPAC drug library [60], DrugBank and PubChem database [61,62] and Traditional Chinese Medicine Systems Pharmacology (TCMSP) database and analysis platform [63]. In addition to these, some specific herbs and natural compounds in the Traditional Chinese Medicine have been attracted by the researchers and several computational studies have been reported. In a screening study of natural compounds, which were taken from Traditional Chinese Medicine System Pharmacology database, 13 antiviral molecules were found to have inhibitory feature against SARS-CoV-2 activity [64]. In other computational studies, inhibitory potency of several antiviral molecules taken from specific herbs or a group of derivatives were tested against SARS-CoV-2. Molecules of Saikosaponins [65], a group of oleanane derivatives, and compounds from *Rhizoma polygonati* [66] and *Glycyrrhiza glabra* [67] were found to have inhibitory capability against SARS-CoV-2. Additionally, glycyrrhizic acid [68], quercetin, isoquercitrin, astragaloside IV and rutin have been reported [69] as effective candidate compounds against SARS-CoV-2.

In the present work, we examined inhibitory potency of natural antiviral compounds published in the Encyclopedia of Traditional Chinese Medicines (ETCM) [70] for S protein, ACE2 and NRP1 receptors. To develop a ligand library for docking, 3D structures of antiviral compounds were obtained from various online databases. However, some of them could not be found and they were prepared by drawing and optimizing their 3D structures with LigPrep module of Maestro [71]. To explore their potential druggability, molecular docking studies were performed to identify compounds that have high binding affinity in the pocket of each receptor. Some of the screened antiviral compounds especially prepared ones produced better docking scores compared to the broad spectrum antivirals such as remdesivir, lopinavir [72,73] when they were docked with S protein. Therefore, natural antiviral compounds identified in this study can be potential therapeutics against

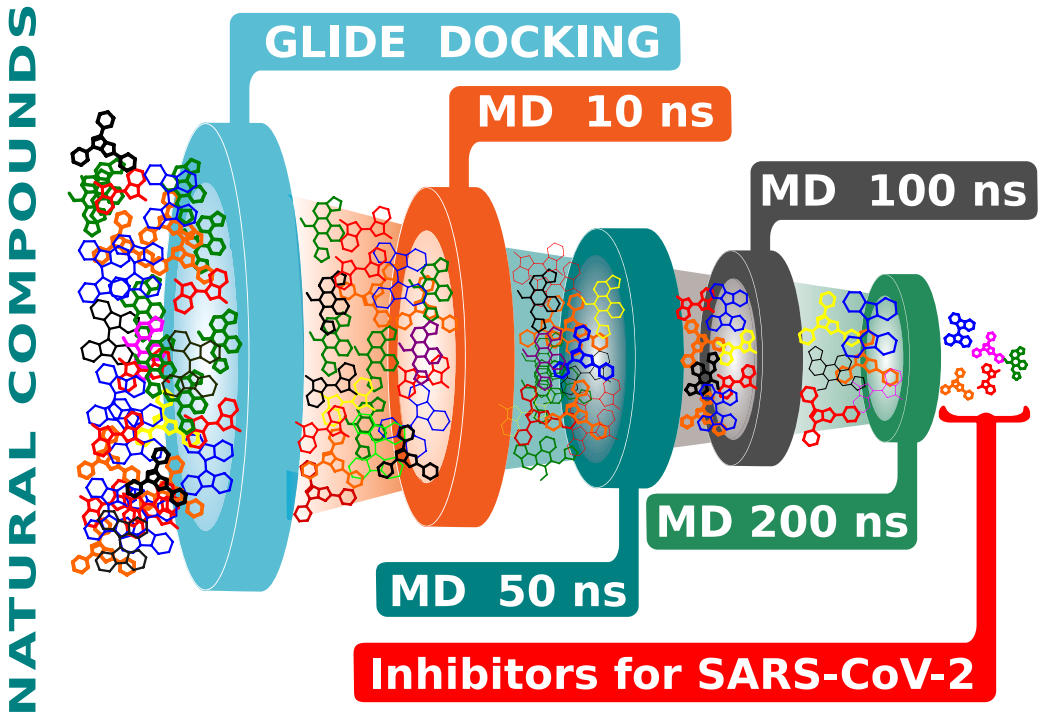

Fig. 2. The approach of searching best inhibitors at the current study.

COVID-19. To verify their docking stability and explore their molecular interactions with the receptors (S protein, ACE2 and NRP1), molecular dynamics simulations were carried out for each compound-receptor complex.

2. Materials and methods

2.1. Ligand preparation

Drug candidates were selected among antiviral compounds from the ETCM [70]. To the best of our knowledge, some of the antiviral molecules in the ETCM have not previously been studied, and they were not published in drug compound data banks. Thus, some of the compounds (see Table S1) have been prepared in 2D form. Then, 3D conformers of ligands with acceptable bond length and angles were generated from their 2D structures using OPLS3e force field and charges [74]. All possible protonation and ionization states were enumerated for each ligand using Epik [75–77] at a pH of 7.2. Only the lowest energy conformer was kept for the docking computation [71].

2.2. Determination of pharmacokinetic properties of ligands

The pharmacokinetic properties of the prepared ligand molecules were determined using the QikProp [78] module in Maestro. Their pharmacokinetic properties and druggability were determined via drug-likeness and bioactivity parameters (donorHB, accptHB, QplogPo/w, QplogHERG, QPPCaco, QPPMDCK, Human Oral Absorption, Percent Human Oral Absorption and Lipinski's rule of five).

2.3. Protein preparation

Crystal structures of SARS-CoV-2 S protein RBD bound with ACE2 (PDB ID: 6M0J) and NRP1 b1 domain in complex with SARS-CoV-2 S1 C-end rule (CendR) peptide (PDB ID: 7JJC) were downloaded from the RCSB web service. As the modeling complex structure of SARS-CoV-2 S protein bound with ACE2 receptor, we chose 6M0J because the structure quality of 6M0J was better than the other ACE2/S protein complexes [79]. Hydrogen atoms, partial charges and side chains and/or whole loop segments are missing in these structure files. Therefore, we processed the structure with the Protein Preparation Wizard [80] in Maestro. Missing atoms and residues were added, and incomplete loop segments were completed using Prime [81–83]. Hydrogen atoms were added after removing any original ones, and bond order adjustment for amino acid residues and ligands was performed. The protonation were adjusted to obtain a pH of 7.2. Water molecules on the active sites and within the distance of 5 Å to the ligands were kept and the others were removed to reduce the computation time. Hydrogen bond sampling with the adjustment of active site water molecule orientations was performed using PROPKA at pH of 7.2. Finally, the protein complexes were subjected to geometry refinement using OPLS3e force field [74] to avoid steric clashes until restrained minimization with convergence of heavy atoms reach to an RMSD of 0.3 Å [84].

2.4. Grid preparation

The receptor grid for targets was prepared using the OPLS3e force field for each structure. We specified the active sites of 6M0J for SARS-CoV-2 as the receptor binding pocket. These active sites include receptor binding motifs of S protein (K417, G446, Y449, Y453, L455, F456, A475, F486, N487, Y489, Q493, G496, Q498, T500, N501, G502, Y505) and peptidase domain (Q24, T27, F28, D30, K31, H34, E35, E37, D38, Y41, Q42, L79, M82, Y83, N330, K353, G354, D355, R357, R393) of ACE2 protein [54]. For 7JJC, active site was chosen around the binding pocket of NRP1 b1 ectodomain (N300, D320, Y297, Y353, T349 and W301) [56]. Softening potential of non-polar atoms of the receptor was performed by scaling the Van der Waals radii by a factor of 1.0. Atoms were considered non-polar if their absolute partial atomic charges were less than or equal to 0.25. The grid center was set to be centroid of active site area and the cubic grid has a side length of 20 Å. No constraints were used in any of the receptor binding regions but rotations were allowed in any of the receptor grids.

2.5. Docking ligands to grids

Prepared ligands were docked into the generated receptor grids using Glide [85–88] with XP docking precision in Maestro. For the docking runs, a softening potential was considered using scaling factor of 0.8 for Van der Waals radii of the ligand's non-polar atoms with an absolute partial atomic charge cut-off of 0.15, which are default values. All poses were subjected to a post-docking minimization. We considered the best-docked structure of the ligand based on the docking score lower (better) than −5.0 kcal/mol [89], which combines the energy grid score, the binding affinity, the internal strain energy, and the Coulomb-Van der Waals interaction energy scores, for the molecular dynamics simulations.

2.6. System preparation

Each system was solvated in an octahedral box using SPC water models [90–92] with at least 10 Å between protein and box boundaries, and neutralized with Na^+ and Cl^- ions. Additionally, we added salts with a concentration of 0.15 M to get a simulation at near physiological conditions. The OPLS3e force field parameters were used for system preparation using the Desmond system builder in Maestro [93,94].

2.7. Molecular dynamics simulation of system

Energy minimization and heating procedures were completed in several steps with default parameters implemented in the Desmond molecular dynamics. The SHAKE algorithm [95] was used to constrain the length of covalent bonds involving hydrogen atoms, and thus the equation of motion was integrated with a time step of 2 fs. The Nose-Hoover thermostat [96] was implemented to equilibrate the temperature of the system at 310 K. Long-range electrostatic interactions were considered using the particle-mesh Ewald method [97], and non-bonded cut-off distance was limited to 9 Å. All MD stages were carried out without any restraints in the isothermal isobaric (NPT) ensemble with 310 K using Berendsen barostat [98] with a target pressure of 1 bar and pressure coupling a constant of 2.0 ps. All MD runs were performed with Desmond on GPU using OPLS3e force field. To test docking stability of the ligand molecules, first all systems were simulated for 10 ns. After each MD simulation, trajectories and timeline representations of the interactions, such as hydrogen bonds, hydrophobic, ionic and water bridges, were examined visually, and the complexes in which the ligand lost its interactions and contacts with the receptor were identified as unstable systems. Hence, they were eliminated and survived systems were extended to 50, 100 and 200 ns (see Fig. 2).

2.8. Analysis of the results

Root mean square deviation (RMSD) of Cα atoms with respect to the initial crystal structure was calculated as a function of time to assess the conformational stability of the protein-ligand complex during the 200 ns MD simulation. Protein-ligand interactions like hydrogen bonds, hydrophobic and ion pair interactions, water bridges, and various structural analysis like root mean square fluctuations (RMSF), principal component analysis based on essential dynamics approach, intermolecular hydrogen bonding and solvent-accessible surface area (SASA) were monitored from the last 100 ns of each MD simulation.

3. Results and discussion

SARS-CoV-2 viral infection starts after the formation of viral binding between the S protein and ACE2 receptor. To prevent infection, proper inhibitors for S protein and ACE2 receptor must be docked with receptor binding domains of S protein and peptidase area of ACE2 receptor, respectively. On the other hand, infectivity of SARS-CoV-2 increases,

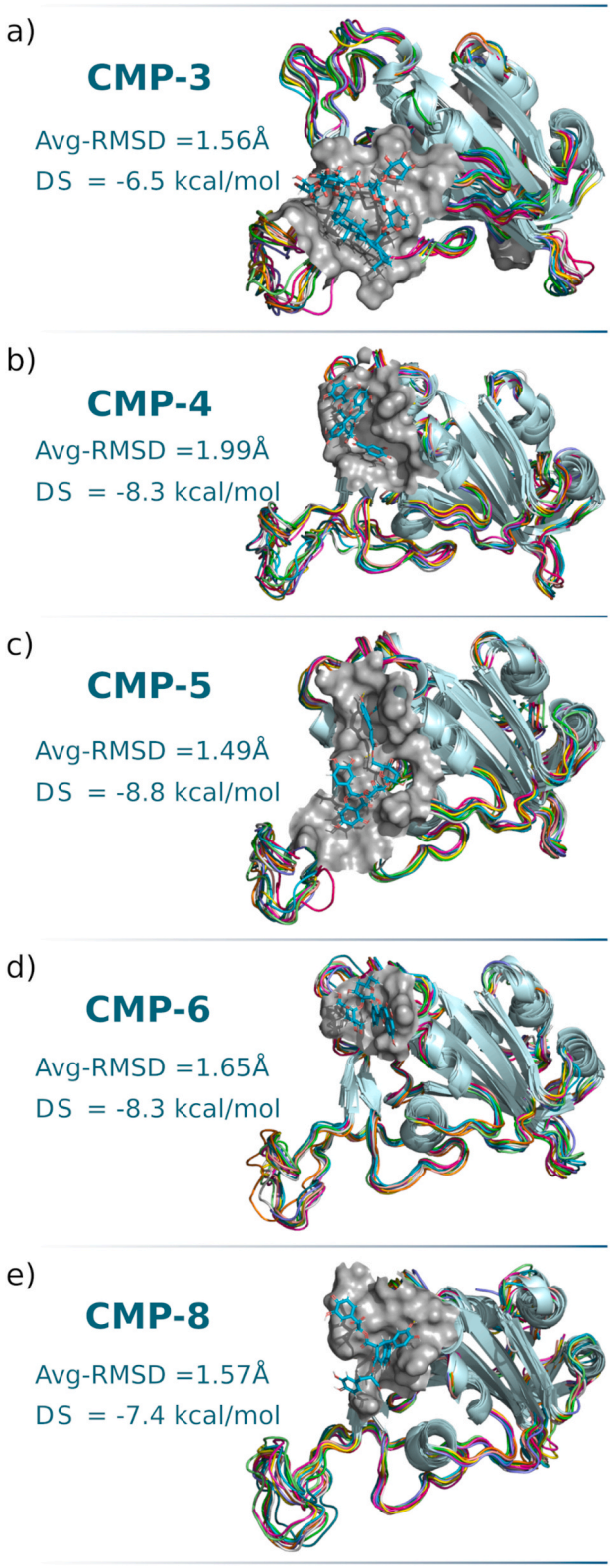

Fig. 3. Superpositions of S protein with CMP-3, CMP-4, CMP-5, CMP-6 and CMP-8. The superposition image of the structure was created from snapshots taken along the trajectory at every 10 ns with PyMol program [99]. Helix residues are indicated in light blue for all snapshots. However, loop residues are indicated in different colors for every snapshot. Abbreviations: Avg-RMSD, Average RMSD; DS, Docking Score. (For interpretation of the references to color in this figure legend, the reader is referred to the Web version of this article.)

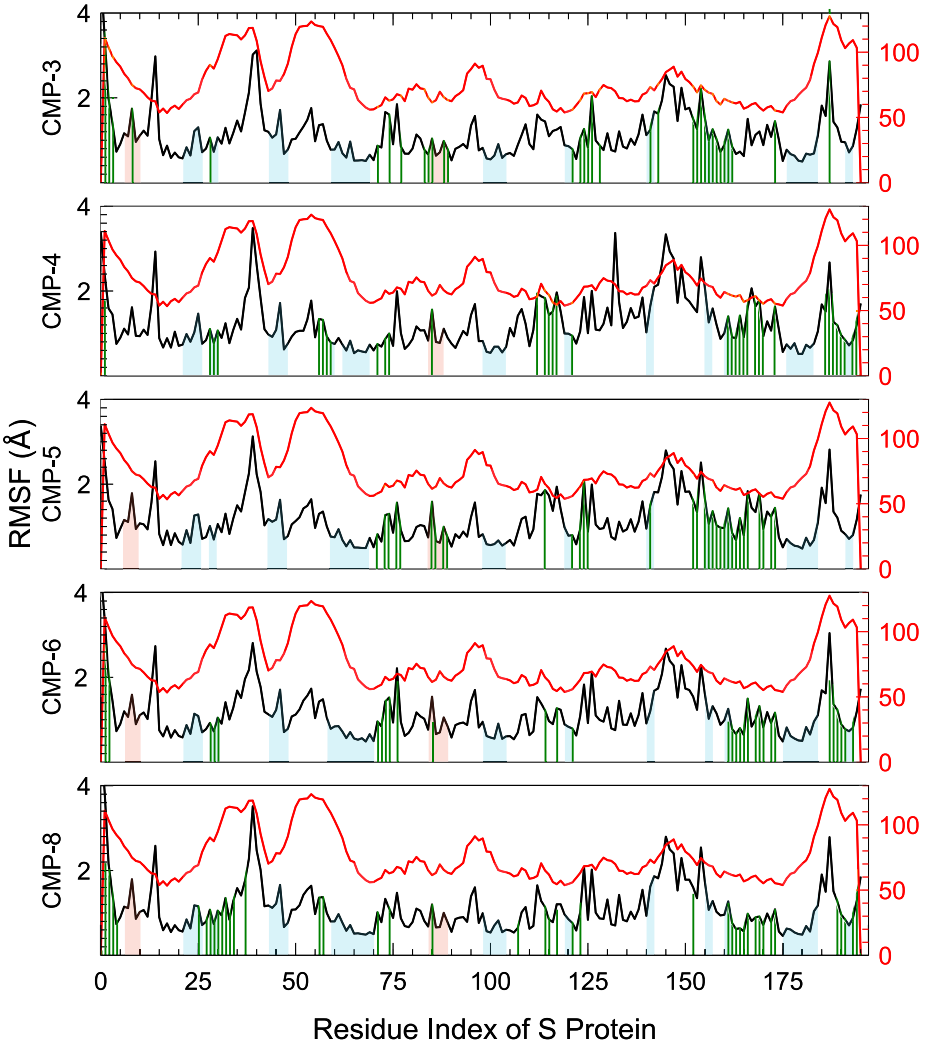

Fig. 4. RMSF plots of S protein with five different compounds. Thick vertical light blue and pink bars below the RMSF values show β-strand and α helices regions of the S protein, respectively. Green vertical lines indicate the residues that interact with compounds. Red plot shows temperature factor of the S protein crystal structure. (For interpretation of the references to color in this figure legend, the reader is referred to the Web version of this article.)

when C-end rule motif of S protein binds to the b1 ectodomain of NRP1 receptor. Therefore, blocking of b1 ectodomain of NRP1 is another important approach to reduce the SARS-CoV-2 infection. Thus, we developed a ligand library from the 374 natural compounds with potential antiviral activities published in the ETCM. First, to determine docking scores and poses of ligands targeted to S protein of SARS-CoV-2, ACE2 and NRP1 receptors, Glide docking [85], an efficient, but less accurate method, was used. After docking, each ligand-receptor system, which includes protein with the natural compound that has the best docking scores, was further evaluated via molecular dynamics simulation method, which is a more accurate, but less efficient computational approach.

3.1. Docking results

To test inhibitory capability of compounds, we docked them with the RBD of SARS-CoV-2 S protein, peptidase area of the ACE2 receptor and b1 ectodomain of NRP1 receptor (see Table S2). Compound poses, which have docking scores lower than −5 kcal/mol with Glide XP precision, were considered for further studies. Some of the screened molecules had more than one docking poses that have nearly equal docking scores with a little structural translation and rotation in their pockets. Therefore, only the one with the lowest docking score was considered for the computation. For S protein, 108 different docking poses were obtained from 62 unique ligands. As mentioned earlier, some of the compounds in our ligand library created from antiviral compounds published in the ETCM, were not found in common online drug/compound libraries, so they were employed to the computation after drawing and optimizing their 3D structures with LigPrep module of Maestro [71]. For S protein, 19 compounds are among the ligands prepared from their 2D forms. For ACE2 receptor, 24 different poses from 18 unique ligands were selected and three of them were among the prepared ligands. Finally, for NRP1, 274 different poses from 81 unique ligands were obtained and 11 compounds were among the prepared ligands. Some of the screened antiviral compounds especially prepared ones produced better docking scores compared to the broad spectrum antivirals such as remdesivir and lopinavir [72,73] (see Figure S1) when they were docked with S protein. Thus, these antiviral compounds identified after docking computation need to be studied further with molecular dynamics simulations techniques whether they are potential therapeutics against COVID-19.

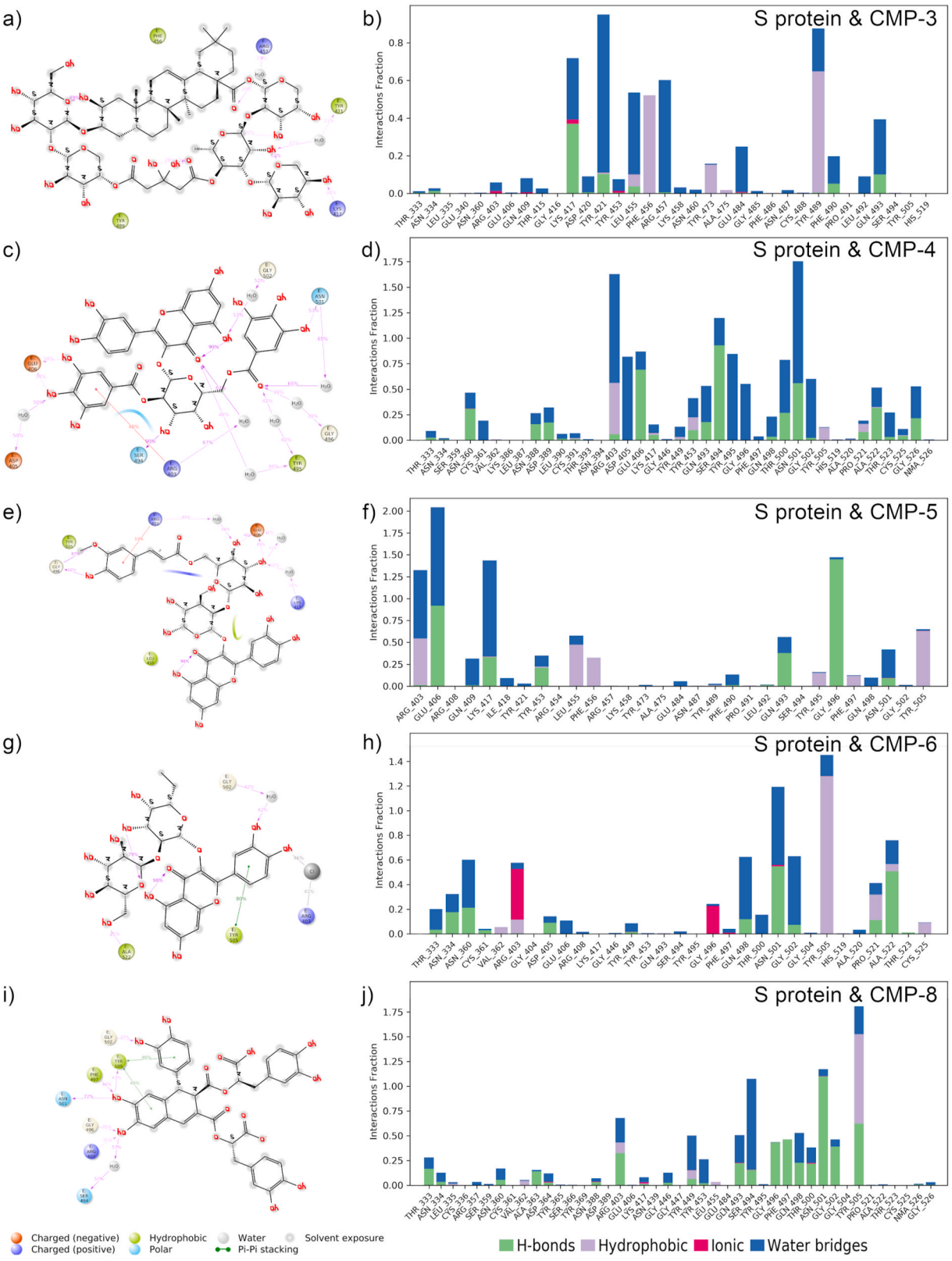

Fig. 5. Protein-ligand interactions for RBD of S protein with (a–b) CMP-3, (c–d) CMP-4, (e–f) CMP-5, (g–h) CMP-6 and (i–j) CMP-8, extracted from the last the 100 ns MD simulations.

3.2. MD results for S protein

3.2.1. RMSD and RMSF

To determine the degree of conformational changes in the protein structure, RMSD of Cα atoms of S protein with CMP-3, CMP-4, CMP-5, CMP-6 and CMP-8 were computed from 200 ns simulation trajectories for each protein-ligand complex and their average of RMSDs was found as 1.56, 1.99, 1.49, 1.65 and 1.57 Å, respectively (see Figure S2). All

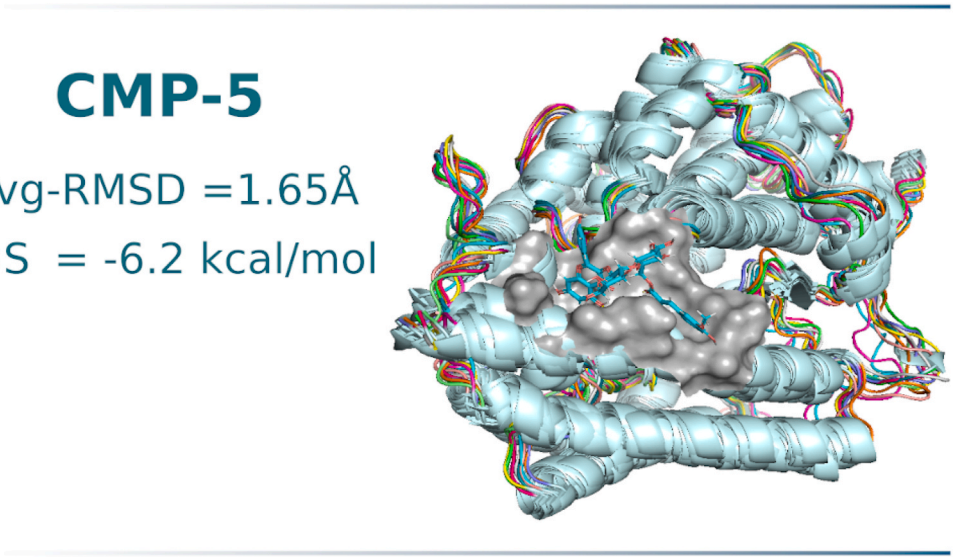

Fig. 6. Most fluxional parts of ACE2 are presented as superpositions of secondary structures for 10 snapshots along the last 100 ns trajectory. Peptidase area within the 5 Å of CMP-5 molecule is shown as gray surface. CMP-5 molecule is presented in ball and stick form. Abbreviations: Avg-RMSD, Average RMSD; DS, Docking Score.

compounds except CMP-4 exhibited RMSDs close to each other, and they have slight deviations from the equilibrium RMSD. On the other hand, CMP-4 has temporary larger RMSD than others especially around 70 ns. However, it is still within an acceptable interval. These RMSDs are within the acceptable range and superposition of each S protein & CMP complex, which were generated from 10 equally separated snapshots from the trajectory of last 100 ns MD simulation, presented in Fig. 3. These indicate that S protein docked with the hit natural compounds showed a persistent conformational stability during the MD simulation.

Root mean square fluctuation (RMSF) shows the individual fluctuations of residues, and it is useful to assess the flexibility of local residues. Therefore, to analyze the stability of complexes, we computed RMSF for each complex considering their heavy atoms, and results with corresponding secondary structures are presented in Fig. 4 β-strands and α-helices always showed lower fluctuations than the loops did, as they are the most motile regions (see Fig. 3). Average RMSF of each complex are below 2 Å, and correlations between RMSF and temperature factor were plotted from their initial crystal structures mostly maintained throughout the last 100 ns MD simulation. All natural compounds did contact mainly with the residues (numbers: 150–175). However, CMP-8 had more contacts with RBD of S protein, especially in two different locations (residue numbers: 25–35, 160–175), than the other compounds.

3.2.2. Molecular interactions

Interactions between S protein and CMP-3 are illustrated in Fig. 5a and b. Residues Glu484, Phe490, Leu492 and Gln493 had hydrogen bond interactions with CMP-3 before MD simulation (see Figure S3). Nonetheless, they lost their interactions immediately at the beginning of MD simulation. On the other hand, residue Lys417 constructed hydrogen bond interactions with the hydroxyl group of tetrahydropyran rings of CMP-3 at least 30% of the simulation time, and it had also considerable water bridges with the CMP-3. Additionally, a few water bridge formations between residues Tyr421 and Arg457, and CMP-3 were detected. Moreover, residues Phe456 and Tyr489 have considerable amount of hydrophobic interactions with CMP-3. Binding affinity between ligand and protein is regulated mainly by hydrogen bond pairings rather than weak interactions such as $\pi - \pi$ stacking, hydrophilic and hydrophobic interactions [100]. Therefore, we addressed residues having hydrogen bond interactions with compounds. Hence, the residue Lys417 was identified as a key residue in the formation of S protein & CMP-3 complex.

Fig. 5c and d shows interactions between residues of S protein with CMP-4. Residues Arg403, Ser494 and Asn501 had hydrogen bond interactions with CMP-4 in the docking pose (see Figure S4). π-cation interactions of residue Arg403 and hydrogen bonding of residue Ser494 with CMP-4 were retained for 48% and 90% of the simulation time, respectively. Additionally, hydrogen bond interactions between residue Arg403 and CMP-4 during the docking pose were altered to water bridge formations with the same oxygen atom of the 4H-chromen-4-one ring. On the other hand, residue Asn501 continued its hydrogen bond interactions with a different 3-hydroxyl benzene moiety for 53% of the simulation time. Additionally, residues Asn501, Tyr495 and Gly496 established water bridges with the oxygen atom of the same moiety of CMP-4 for 65%, 42% and 39% of the simulation time, respectively. On the other hand, residue Glu406 formed hydrogen bond interactions with two of hydroxyl groups, and residue Asp405 also constructed water bridges with the second hydroxyl group of the other p-hydroxy group of trihydroxybenzoate. Residues Arg403 and Tyr495 constructed water bridges with the same oxygen atom of 4H-chromen-4-one moiety of CMP-4 for 67% and 40% of the simulation time, respectively. Moreover, residue Gly502 established water bridges with the hydroxyl group of the same moiety for 52% of the simulation time. Hence, residues Arg403, Glu406 and Asn501 were identified as key residues in the formation of S protein & CMP-4 complex.

Interactions between S protein and CMP-5 are displayed in Fig. 5e and f. Residues Glu406 and Gly496, which had hydrogen bond interactions in the docking pose (see Figure S5), retained their interactions with CMP-5 for 46% and 87% of the simulation time, respectively. Residue Gly496 also constructed new hydrogen bond interactions with the hydroxyl group of the same moiety for 56% of the simulation time. However, residue Lys417 exhibited water bridge interactions mainly instead of hydrogen bond interactions for 32% of the simulation time. Residue Arg403 established π-cation interactions with 2-methoxyphenol ring and water bridge with the adjacent tetrahydropyran ring for 53% and 44% of the simulation time, respectively. Additionally, a water bridge formation, which has a connection between residue Glu406 and hydroxyl group of tetrahydropyran ring, has been observed for 31% of the simulation time. Consequently, residues Gly496 and Glu406 were identified as key residues in the formation of S protein & CMP-5 complex.

Fig. 5g and h shows interactions between residues of S protein with

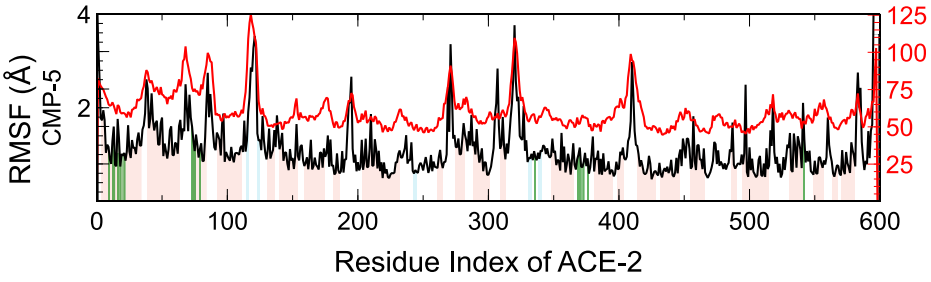

Fig. 7. RMSF plot of ACE2 with CMP-5. Thick vertical light blue and light pink bars below the RMSF values show β-strand and α-helices of the ACE2, respectively and green vertical lines indicate residues that interact with CMP-5. Red plot shows temperature factor of the ACE2 crystal structure. (For interpretation of the references to color in this figure legend, the reader is referred to the Web version of this article.)

CMP-6. Hydrogen bond interactions of residues Gly446, Gln493, Ser494, Gly496 and Tyr505, and π-cation interactions of Arg403, which were observed in the docking poses (see Figure S6), did not retain their interactions with CMP-6 in the course of MD simulation. However, residue Ala522 established hydrogen bond interactions with the hydroxyl group of tetrahydropyran ring of CMP-6 for 41% of the simulation time. Additionally, $\pi - \pi$ stacking interactions and water bridge formations between residues Gly502 and Tyr505, and 1,2-dihydroxybenzene moiety of CMP-6 were observed for 80% and 42% of the simulation time, respectively. Moreover, an ion bridge interactions through a Cl^- ion were established between Arg403 and the other hydroxyl group of the same moiety for 46% of the simulation time. Hence, residues Tyr505 and Ala522 were identified as key residues in the formation of S protein & CMP-6 complex, and residues Arg403 and Gly502 also play an important role in this complex with their ion and water bridge formations, respectively.

Fig. 5i and j shows interactions between residues of S protein with CMP-8. Although Glu406, Gln409, Lys417, Gln493 and Tyr505 had hydrogen bond interactions with CMP-8 in the docking poses (see Figure S7), only the residue Tyr505 continued its hydrogen bond interactions and $\pi - \pi$ stacking interactions with adjacent 1,2-dihydroxybenzene ring for 41% and 40%of the simulation time, respectively. Additionally, other $\pi - \pi$ stacking interactions (46%) with adjacent 1,2-dihydroxybenzene ring was established. Furthermore, hydrogen bond interactions were observed between residue Gly502 and the same group for 37% of the simulation time. On the other hand, hydroxyl groups of the 1,2-dihydroxybenzene ring were attracted by the surrounding residues Arg403 (31%), Gly496 (35%), Phe497 (46%), Asn501 (72%) and Tyr505 (41%). However, only water bridge interactions were observed between Ser496 and CMP-8 for 57% of the simulation time. Hence, residues Asn501, Phe497, Tyr505, Gly502, Gly496 and Arg403 were identified as key residues in the formation of S protein & CMP-8 complex.

3.3. MD results for ACE2 receptor

3.3.1. RMSD and RMSF

Among the compounds subjected to MD simulations, only the ACE2 & CMP-5 receptor complex was survived after 200 ns MD simulation. RMSD was computed from the Cα atoms of ACE2 receptor. The average RMSD of the Cα atoms was found 1.64 Å, and it is within the acceptable range (see full RMSD graph in Figure S8). To obtain further information about deviations on the structure, a superposition (see Fig. 6) was generated from 10 equally separated snapshots from the trajectory of the last 100 ns MD simulation (i.e., consecutive snapshots have 10 ns time intervals) as it is quite stable.

A plot of the RMSF analysis of ACE2 including interactions of residues with CMP-5 through the last 100 ns MD simulation trajectory is shown in Fig. 7; also, illustrated is a color bar providing the correlation between residues and the secondary structure regions. As seen in Fig. 7, strand residues always have lower RMSF values. On the other hand, loop residues, such as Gln139, Asn338, Tyr613, Ala614 and Asp615, have the largest RMSF values as they are the most motile regions. Their RMSFs show coherence with B-factor of the ACE2 crystal structure. The overall RMSD and RMSF plots of ACE2 & CMP-5 complex imply that the complex tends to be stabilized during the course of the MD simulation.

3.3.2. Molecular interactions

Fig. 8a and b shows residue interactions of ACE2 with CMP-5. During the docking poses, residues Lys26, Ala387 and Arg353 had hydrogen bond interactions with CMP-5 (see Figure S9). MD simulation analysis shows that residue Arg393 retained its hydrogen bond interactions with hydroxyl group of its tetrahydropyran ring for 55% of the simulation time and residue Lys26 continued to form mainly π-cation interactions with 4H-chromen-4-one moiety for 80% of the simulation time in addition to the water bridge formation. However, the residue Ala387 was less likely to retain its interactions. On the other hand, residues Phe390 and Asp38 established significant hydrogen bond interactions with the fragment of CMP-5 for 99% and 84% of the simulation time,

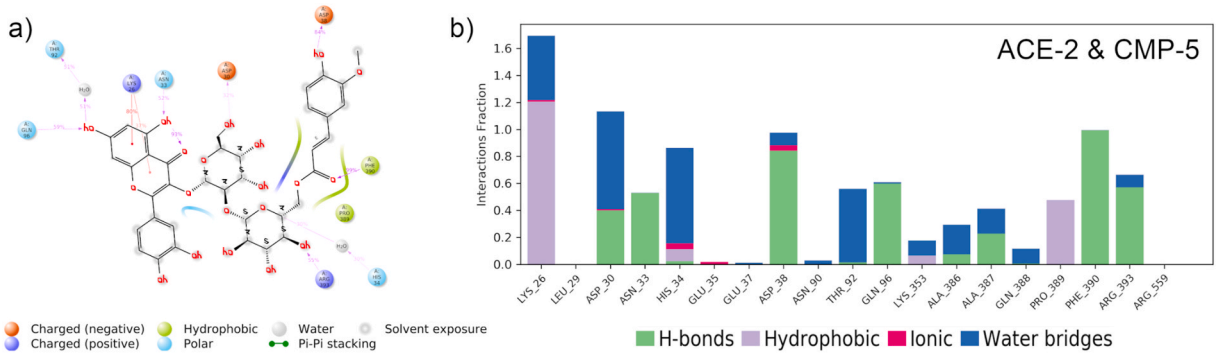

Fig. 8. Protein-ligand interactions for peptidase area of ACE2 with (a–b) CMP-5, extracted from the last 100 ns MD simulations.

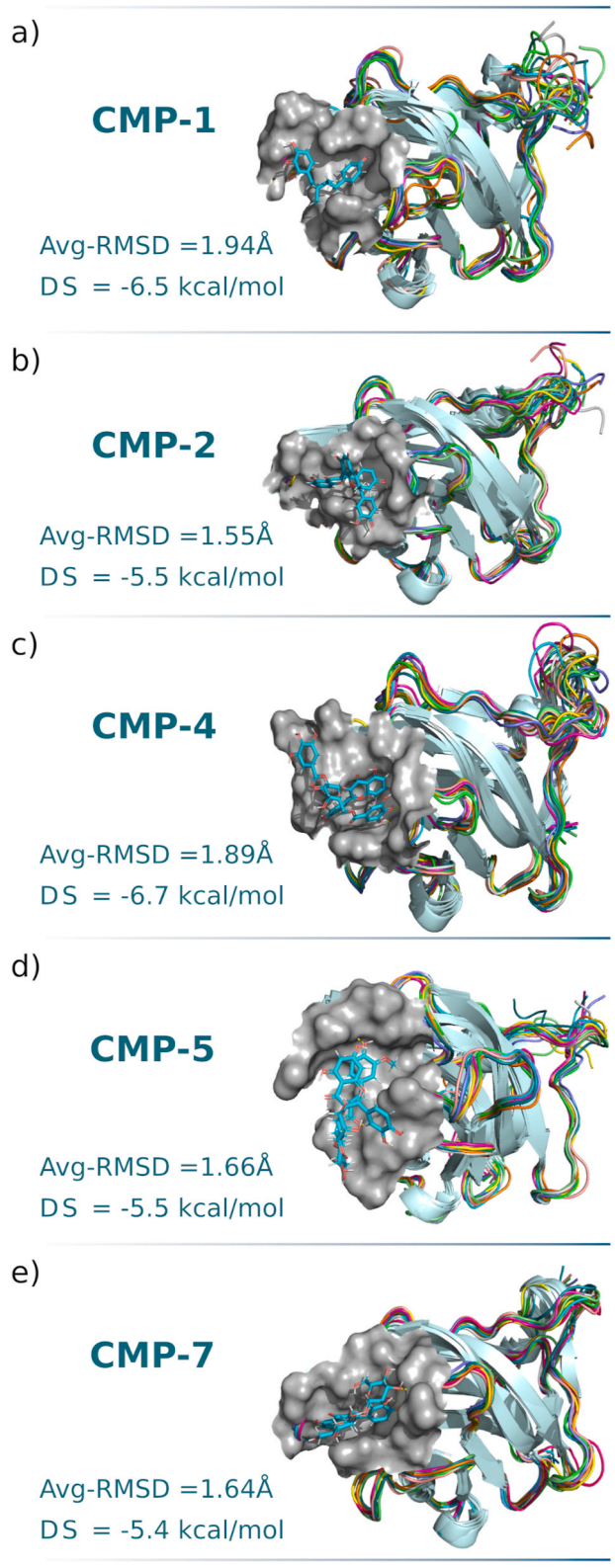

Fig. 9. Superpositions of NRP1 with CMP-1, CMP-2, CMP-4, CMP-5 and CMP-7. Abbreviations: Avg-RMSD, average RMSD; DS, docking score.

respectively. Additionally, residues Asp30, Asn33 and Gln96 had hydrogen bond interactions with its different hydroxyl groups for 32%, 52% and 59% of the simulation time, respectively. Moreover, residues His34 and Thr92 constructed water bridges with its tetrahydropyran and 4H-chromen-4-one for 30% and 51% of the simulation time, respectively. Consequently, residues Phe390, Asp38, Lys26, Gln59, Arg393 and Asp30 were identified as the key residues involved in the formation of ACE2 & CMP-5 complex.

3.4. MD results for neuropilin receptor

3.4.1. RMSD and RMSF

After 200 ns MD simulations, CMP-1, CMP-2, CMP-4, CMP-5 and CMP-7 showed consistent interactions with the b1 ectodomain of the NRP1 receptor, and averages of computed RMSDs from the Cα atoms are 1.94, 1.55, 1.89, 1.66 and 1.64 Å, respectively (see Figure S10). Their superpositions (see Fig. 9) were generated from 10 equally separated snapshots from the trajectory of the last 100 ns MD simulation of each complex. Higher flexuous RMSD were observed in the CMP-1 and CMP-2 complexes than the CMP-4, CMP-5 and CMP-7 complexes, which are quercetin derivatives.

Fig. 10 shows RMSF analysis of the last 100 ns MD simulation trajectory for NRP1 including residues interacting with CMP-1, CMP-2, CMP-4, CMP-5 and CMP-7. N-tail of the NRP1 protein (first residues) has longer loop region than the C-tail (last residues) does. Therefore, significant fluctuations have been observed in the N-tail than the C-tail of the protein in each MD simulation of the complex. All residues (numbers: 36–40, 52, 55–59, 85–88, 90, 92 and 152–154), which are accumulated mainly in four different locations on the RMSF charts (see Fig. 10), did contact with the natural compounds in all MD simulations. Particularly, the CMP-5 did more contacts with the NRP1 receptor than the other compounds did.

3.4.2. Molecular interactions

Fig. 11a and b shows residue interactions of NRP1 with CMP-1. It shows that among the interactions of residues Ser298, Asn300, Trp301 and Asp320 with CMP-1 computed during the docking section (see Figure S11), only interactions between Asp320 (47%) and phenol ring of CMP-1 were retained for more than 30% of the simulation time. However, new hydrogen bond formations, which retained for 31% of the simulation time, were observed between the residue Glu348 and two hydroxyl groups of 1,2-dihydroxybenzene moiety, which was occupied previously by residues Ser298 and Asn300. Additionally, residue Trp301 that has a hydrophobic contact in the form of $\pi - \pi$ interaction before the simulation rarely established hydrogen bonds with one of the same hydroxyl group. However, residues Tyr297 and Tyr353, which have hydrophobic interactions before the MD simulation, continued to form hydrophobic interactions considerably with the CMP-1. Both residues Asp320 and Glu348 were involved in the water bridge formation considerably (see Fig. 11a and b) during the simulation. Hence, these residues Tyr297, Trp301, Asp320, Glu348 and Tyr353, some of which were defined as active residues in the ectodomain of NRP1 [56], were identified as the key residues involved in the formation of NRP1 & CMP-1 complex.

Residue interactions of NRP1 with CMP-2 were shown in Fig. 11c and d. Interactions between residues Tyr297, Trp301 and Asp320, and CMP-2 computed during the docking stage were conserved for more than 30% of the simulation time. The residue Tyr297 had hydrogen bond and $\pi - \pi$ interactions with the oxygen atom of 4H-chromen-4-one and the 1,2-dihydroxybenzene moiety of CMP-2, respectively, during the docking stage (see Figure S12), but only $\pi - \pi$ interactions with the 1,2-dihydroxybenzene moiety were survived for 52% of the simulation time. Additionally, a considerable number of water bridge formations were observed between the residue Tyr297 and two hydroxyl groups of the 1,2-dihydroxybenzene moiety of CMP-2 (see Fig. 11d). Residues Trp301 and Asp320 formed hydrogen bonds with the hydroxyl groups of 4H-chromen-4-one and phenol ring of CMP-2 for 42% and 53% of the simulation time, respectively. Moreover, a few water bridge formations were observed between residue Asp320 and CMP-2. On the other hand, residue Glu348, which did not show any interaction with CMP-2 during the docking stage, established hydrogen bond with the hydroxyl group

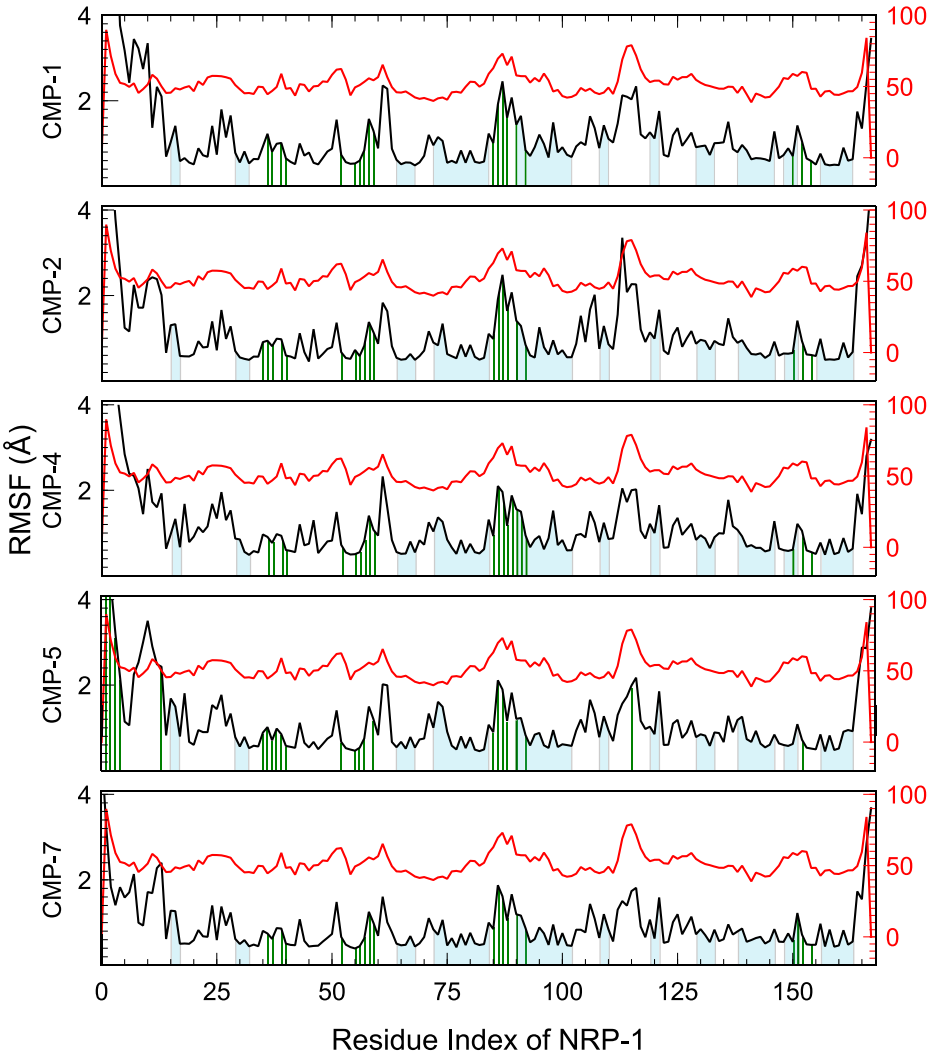

Fig. 10. RMSF plots of NRP1 with five different compounds. Light blue areas below the RMSF values show β-strand regions of NRP1 and green vertical lines indicate residues that interact with compounds. Red plot shows temperature factor of the NRP1 crystal structure. (For interpretation of the references to color in this figure legend, the reader is referred to the Web version of this article.)

of 4H-chromen-4-one moiety for 44% of the simulation time. Consequently, residues Tyr297, Trp301, Asp320 and Glu348 were identified as the key residues involved in the formation of NRP1 & CMP-2 complex.

Figs. 11e and f shows residue interactions of NRP1 with CMP-4. Molecular interactions (see Figure S13), formed before MD simulation were not retained as MD computation started, and new molecular interactions were established between the residues and CMP-4. Thr316, Pro317, Asp320, Glu348 and Ile415 have interactions with CMP-4 for more than 30% of the simulation time. Especially, residue Asp320 established strong interactions with two hydroxyl groups of the trihydroxybenzoate moiety. Moreover, a water bridge, which existed about 63% of the simulation time, occurred between the residue Asp320 and CMP-4. The residue Pro317 constructed hydrogen bonds with the other hydroxyl group of the same trihydroxybenzenes moiety for 79% of the simulation time. Residues Thr316 and Ile415 formed hydrogen bonds with the same hydroxyl group of the 4H-chromen-4-one moiety for 75% and 32% of the simulation time, respectively. Another important hydrogen bond formation was observed between the residue Glu348 and the hydroxyl group of the 1,2-dihydroxybenzene moiety for 57% of the simulation time. Hence, residues Thr316, Pro317, Asp320, Glu348 and Ile415 were identified as the key residues involved in the formation of NRP1 & CMP-4 complex.

Important residue interactions of NRP1 with CMP-5 were depicted in Fig. 11g and h. Hydrogen bonds were observed between residues (Asn300, Asp320 and Tyr353) and CMP-5 during docked poses (see Figure S14). Only the residue Tyr353 conserved its interaction with CMP-5, but it established hydrogen bonds with the hydroxyl group of the different moiety for 85% of the simulation time. Additionally, Thr349 established an interaction via hydrogen bond formation with the same hydroxyl group for 52% of the simulation time. Although residue Asn300 continued a few water bridges and hydrogen bond formations during the MD simulation, the residue Asp320 did not retain any interaction with CMP-5. Interestingly, residue Ser298 established an enduring interactions with CMP-5 via hydrogen bonding with the oxygen atom of CMP-5 for 98% of the simulation time. Therefore, residues Ser298, Thr349 and Tyr353 were identified as the key residues involved in the formation of NRP1 & CMP-5 complex.

Interactions of residues of NRP1 with CMP-7 are presented in Fig. 11i and j the residues Tyr297, Ser298 and Asp320 had hydrogen bonding with CMP-7 at initial docked poses (see Figure S15). Only the residue Asp320 continued to interact with CMP-7 during the course of MD simulation. However, residue Asp320 established significant hydrogen bond formations with the next two hydroxyl group of the same moiety for 97% and 77% of the simulation time. Residues Trp301 and Glu348

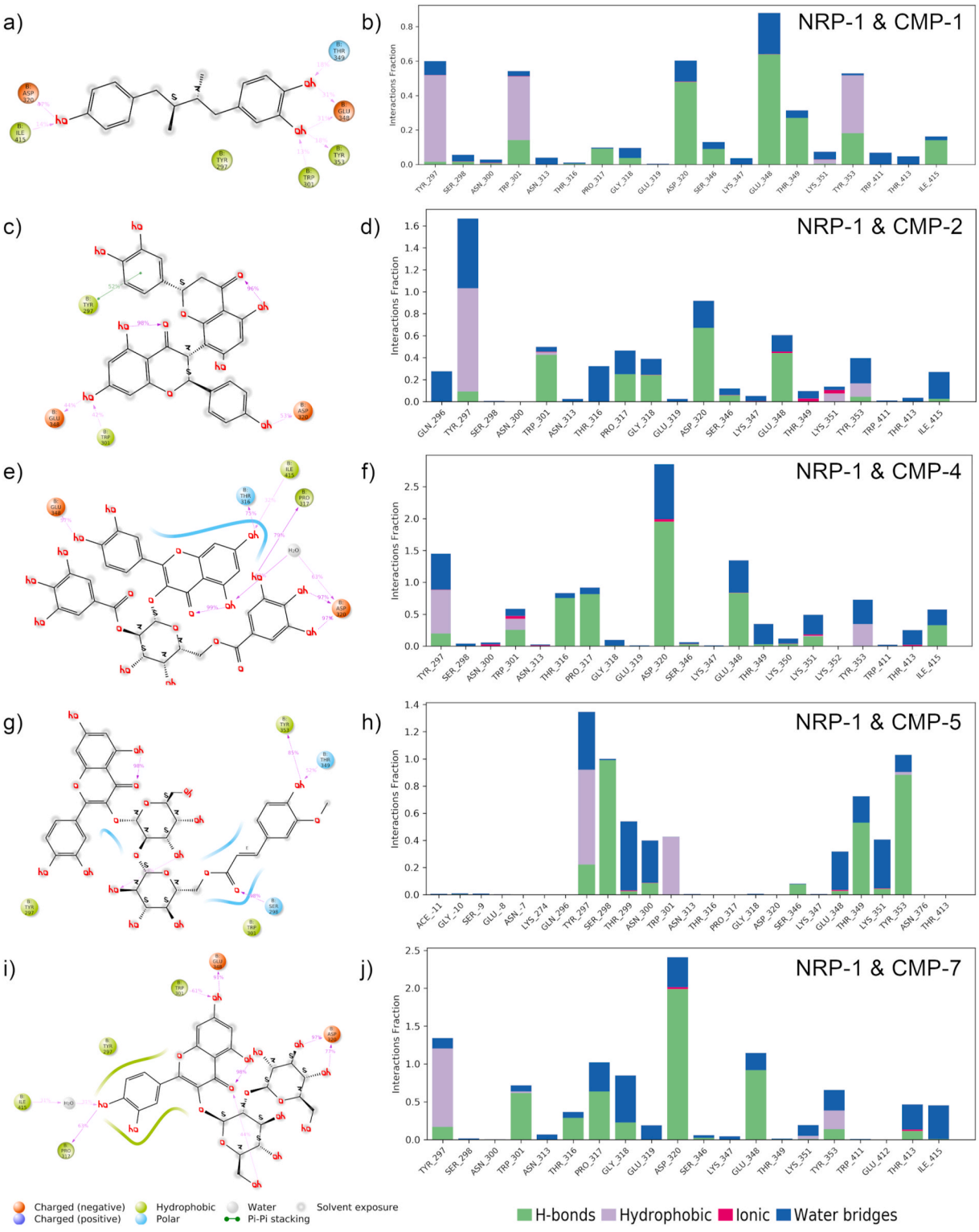

Fig. 11. Protein-ligand interactions for b1 ectodomain of NRP1 with (a–b) CMP-1, (c–d) CMP-2, (e–f) CMP-4, (g–h) CMP-5 and (i–j) CMP-7, extracted from the last 100 ns MD simulations.

established hydrogen bonds with the same hydroxyl group for 61% and 91% of the simulation time, respectively. Additionally, residue Pro317 formed hydrogen bond interaction with the hydroxyl group of the 1,2-dihydroxybenzene moiety for 63% of the simulation time. Moreover, the residue Ile415 interacted with the same hydroxyl group via forming water bridges for 31% of the simulation time. Hence, residues Trp301, Pro317, Asp320 and Glu348 were identified as the key residues involved in the formation of NRP1 & CMP-7 complex.

Even though some of the compounds in our library produced significantly lower docking scores, most of them did not show a persistent binding stability and detached from their binding pockets during the MD simulations. Molecules identified as strong binders have various functional group of atoms, especially aromatic rings with O–H groups. Lower docking scores could be produced thanks to these O–H

Table 1
Eight hit compounds found effective for inhibition of NRP1, ACE2 receptors or S protein of SARS-CoV-2 after docking computation and molecular dynamics simulations. Their names, pharmacological activities and natural sources are also tabulated [70].

[1.5 pt] **Name**	**Pharm. Activities**	**Natural Sources**
CMP-1	Anti-HIV	*Larrea tridentata*
CMP-2	Anti-HIV-1 (RT inh.), Anti-EBV, Antioxidant	*Garcinia multiflora, Garcinia dulcis*
CMP-3	Anti-HSV-1	*Bolbostemma paniculatum*
CMP-4	HIV-1 (IN inh.)	*Acer okamotoanum*
CMP-5	Anti-HIV-1 (RT and IN inh.), Neuroprotective	*Thevetia neriifolia, Oldenlandia diffusa*
CMP-6	Anti-HIV-1 (RT and IN inh.), Neuroprotective, DDDP inh.	*Oldenlandia diffusa, Thevetia neriifolia*
CMP-7	Anti-HIV-1 (RT and IN inh.), DDDP inh.	*Thevetia neriifolia, Apocymum venetum*
CMP-8	Anti-HIV	*Lithospermum erythrorhizon, Amebia euchroma*

Abbreviations: HIV, Human Immunodeficiency Virus; RT, Reverse Transcriptase; EBV, Epstein-Barr Virus; DDDP, DNA-dependent DNA polymerase; IN, Integrase; inh, Inhibitor.

groups that involved in the formation of hydrogen bonding with residues of the receptor, which is one of the major parameters to score docking. As seen in Table 1, eight compounds have shown to have antiviral activity against HIV, EBV or HSV. Four of them identified as inhibitors for NRP1, ACE2 and S protein are quercetin derivatives which have antiviral property.

Quercetin, which is a flavonoid compound found abundantly in vegetables and fruits, was reported to have antiviral activity against various viruses such as Influenza [101,102] and EBOLA [103] viruses, HIV-1 [104] and MERS-CoV [105]. Common forms of quercetin also showed a good inhibitory activity against SARS-CoV [106,107] and SARS-CoV-2 [108]. Furthermore, various *in-silico* and clinical studies based on various quercetin therapeutics were reported in reviews [109,110]. Our computational study showed that some of quercetin molecules taken from ETCM bind strongly to NRP1, ACE2 and S protein, and their binding stability were meticulously tested with long MD simulations. Apart from the common forms of quercetin, molecules in our compound library have some various moieties, and our analysis showed that those moieties have significant non-covalent interactions with the key residues of NRP1, ACE2 and S protein. Therefore, CMP-4, CMP-5, CMP-6 and CMP-7 can have multi inhibitory activity against infection of SARS-CoV-2. Further experimental studies would be critically important to test their potential druggability, especially CMP-5 because it was found effective for all targets. However, when quercetin is taken orally, it interacts with a series of proteins and enzymes as it moves through the gastrointestinal system. Therefore, its absorption is limited significantly [111]. Pharmacokinetic analysis of the CMP-4, CMP-5, CMP-6 and CMP7 (see Table S1) revealed a similar low bioavailability. Hence, these drug candidates could be more efficient when they are used as nasal spray and phytosome [112,113].

4. Conclusions

In summary, we screened natural antiviral compounds published in the Encyclopedia of Traditional Chinese Medicines against ACE2, NRP1 and S protein. Molecular docking of natural antiviral compounds was carried out, and the compounds with less than the docking score of −5 kcal/mol were considered for further studies. Molecular dynamics simulations of compound-receptor complex have been performed up to 200 ns to find the most strong binders. We found CMP-3, CMP-4, CMP-5, CMP-6 and CMP-8 are strong binders for the spike protein, CMP-1, CMP-2, CMP-4, CMP-5 and CMP-7 are strong binders for the neuropilin receptor, and CMP-5 is a strong binder for the ACE2. Quercetin derivatives (CMP-4, CMP-5, CMP-6 and CMP-7) were found highly stable in the active domain of NRP1, ACE2 and S protein. Especially, the CMP-5 showed an inhibitory activity for all targets. Overall, our results provide valuable insights into inhibitory mechanism of natural antiviral compounds on ACE2, NRP1 and S protein, and support for experimental studies.

Funding

This research did not receive any specific grant from funding agencies in the public, commercial, or not-for-profit sectors.

Declaration of competing interest

The authors declare that they have no known competing financial interests or personal relationships that could have appeared to influence the work reported in this paper.

Acknowledgement

We thank Abdurrahman Olgac for partial GPU resources. We also thank Dilara Berna Yıldız for naming compound moieties. We thank Gazi University Directorate of Information Technologies and Academic Writing Center for providing license of Schrödinger Maestro Suit software and their support in revising this manuscript, respectively.

Appendix A. Supplementary data

Supplementary data to this article can be found online at https://doi.org/10.1016/j.jmgm.2021.108038.

References

[1] Pneumonia of unknown cause china-2021. World Health Organization, https://www.who.int/csr/don/05-january-2020-pneumonia-of-unkown-cause-china/en/(accessed Sep 10, 2021).
[2] WHO Coronavirus Disease (COVID-19) Dashboard. World Health Organization, https://covid19.who.int (accessed Sep 10, 2021).
[3] H. Wang, X. Li, T. Li, S. Zhang, L. Wang, X. Wu, J. Liu, The genetic sequence, origin, and diagnosis of SARS-CoV-2, Eur. J. Clin. Microbiol. Infect. Dis. 39 (9) (2020) 1629–1635, https://doi.org/10.1007/s10096-020-03899-4.
[4] E.M. Mangum, K.K. Graham, Lopinavir-ritonavir: a new protease inhibitor, Pharmacotherapy, J.Hum. Pharmacol.Drug Ther. 21 (11) (2001) 1352–1363, https://doi.org/10.1592/phco.21.17.1352.34419.
[5] J. Pasquau, C. Hidalgo-Tenorio, M.L. Montes, A. Romero-Palacios, J. Vergas, I. Sanjoaquín, J. Hernández-Quero, K. Aguirrebengoa, F. Orihuela, A. Imaz, M. J. Ríos-Villegas, J. Flores, M.C. Fariñas, P. Vázquez, M.J. Galindo, I. García-Mercé, F. Lozano, I. de los Santos, S.E. de Jesus, C. García-Vallecillos, On behalf of the QoLKAMON STUDY GROUP, High quality of life, treatment tolerability, safety and efficacy in hiv patients switching from triple therapy to lopinavir/ritonavir monotherapy: a randomized clinical trial, PloS One 13 (4) (2018) 1–15, https://doi.org/10.1371/journal.pone.0195068.
[6] C.M. Chu, V.C.C. Cheng, I.F.N. Hung, M.M.L. Wong, K.H. Chan, K.S. Chan, R.Y. T. Kao, L.L.M. Poon, C.L.P. Wong, Y. Guan, J.S.M. Peiris, K.Y. Yuen, Role of lopinavir/ritonavir in the treatment of sars: initial virological and clinical findings, Thorax 59 (3) (2004) 252–256, https://doi.org/10.1136/thorax.2003.012658.
[7] M.E. Morra, L. Van Thanh, M.G. Kamel, A.A. Ghazy, A.M. Altibi, L.M. Dat, T.N. X. Thy, N.L. Vuong, M.R. Mostafa, S.I. Ahmed, S.S. Elabd, S. Fathima, T. Le Huy Vu, A.S. Omrani, Z.A. Memish, K. Hirayama, N.T. Huy, Clinical outcomes of current medical approaches for middle east respiratory syndrome: a systematic review and meta-analysis, Rev. Med. Virol. 28 (3) (2018), e1977, https://doi.org/10.1002/rmv.1977.
[8] D. Cattaneo, D. Cattaneo, C. Gervasoni, M. Corbellino, M. Galli, A. Riva, C. Gervasoni, E. Clementi, E. Clementi, Does lopinavir really inhibit sars-cov-2? Pharmacol. Res. 158 (2020) 104898, https://doi.org/10.1016/j.phrs.2020.104898.
[9] B. Nutho, P. Mahalapbutr, K. Hengphasatporn, N.C. Pattaranggoon, N. Simanon, Y. Shigeta, S. Hannongbua, T. Rungrotmongkol, Why are lopinavir and ritonavir effective against the newly emerged coronavirus 2019? atomistic insights into the inhibitory mechanisms, Biochemistry 59 (18) (2020) 1769–1779, https://doi.org/10.1021/acs.biochem.0c00160.
[10] M. Vargas, G. Servillo, S. Einav, Lopinavir/ritonavir for the treatment of sars, mers and covid-19: a systematic review, Eur. Rev. Med. Pharmacol. Sci. 24 (16) (2020) 8592–8605, https://doi.org/10.26355/eurrev_202008_22659.

[11] T.-T. Yao, J.-D. Qian, W.-Y. Zhu, Y. Wang, G.-Q. Wang, A systematic review of lopinavir therapy for sars coronavirus and mers coronavirus-a possible reference for coronavirus disease-19 treatment option, J. Med. Virol. 92 (6) (2020) 556–563, https://doi.org/10.1002/jmv.25729.

[12] B. Cao, Y. Wang, D. Wen, W. Liu, J. Wang, G. Fan, L. Ruan, B. Song, Y. Cai, M. Wei, X. Li, J. Xia, N. Chen, J. Xiang, T. Yu, T. Bai, X. Xie, L. Zhang, C. Li, Y. Yuan, H. Chen, H. Li, H. Huang, S. Tu, F. Gong, Y. Liu, Y. Wei, C. Dong, F. Zhou, X. Gu, J. Xu, Z. Liu, Y. Zhang, H. Li, L. Shang, K. Wang, K. Li, X. Zhou, X. Dong, Z. Qu, S. Lu, X. Hu, S. Ruan, S. Luo, J. Wu, L. Peng, F. Cheng, L. Pan, J. Zou, C. Jia, J. Wang, X. Liu, S. Wang, X. Wu, Q. Ge, J. He, H. Zhan, F. Qiu, L. Guo, C. Huang, T. Jaki, F.G. Hayden, P.W. Horby, D. Zhang, C. Wang, A trial of lopinavir–ritonavir in adults hospitalized with severe covid-19, N. Engl. J. Med. 382 (19) (2020) 1787–1799, https://doi.org/10.1056/NEJMoa2001282.

[13] P.W. Horby, M. Mafham, J.L. Bell, L. Linsell, N. Staplin, J. Emberson, A. Palfreeman, J. Raw, E. Elmahi, B. Prudon, C. Green, S. Carley, D. Chadwick, M. Davies, M.P. Wise, J.K. Baillie, L.C. Chappell, S.N. Faust, T. Jaki, K. Jefferey, W.S. Lim, A. Montgomery, K. Rowan, E. Juszczak, R. Haynes, M.J. Landray, Lopinavir-ritonavir in patients admitted to hospital with covid-19 (recovery): a randomised, controlled, open-label, platform trial, Lancet 396 (10259) (2020) 1345–1352, https://doi.org/10.1016/S0140-6736(20)32013-4.

[14] T.-T. Yao, J.-D. Qian, W.-Y. Zhu, Y. Wang, G.-Q. Wang, A systematic review of lopinavir therapy for sars coronavirus and mers coronavirus—a possible reference for coronavirus disease-19 treatment option, J. Med. Virol. 92 (6) (2020) 556–563, https://doi.org/10.1002/jmv.25729.

[15] T. Bhatnagar, M. Murhekar, M. Soneja, N. Gupta, S. Giri, N. Wig, R. Gangakhedkar, Lopinavir/ritonavir combination therapy amongst symptomatic coronavirus disease 2019 patients in India: protocol for restricted public health emergency use, Indian J. Med. Res. 151 (2) (2020) 184–189, https://doi.org/10.4103/ijmr.IJMR_502_20.

[16] Y. Li, Z. Xie, W. Lin, W. Cai, C. Wen, Y. Guan, X. Mo, J. Wang, Y. Wang, P. Peng, X. Chen, W. Hong, G. Xiao, J. Liu, L. Zhang, F. Hu, F. Li, F. Zhang, X. Deng, L. Li, Efficacy and safety of lopinavir/ritonavir or arbidol in adult patients with mild/moderate covid-19: an exploratory randomized controlled trial, Med 1 (1) (2020) 105–113, https://doi.org/10.1016/j.medj.2020.04.001, e4.

[17] B. Morgenstern, M. Michaelis, P.C. Baer, H.W. Doerr, J. Cinatl, Ribavirin and interferon-beta synergistically inhibit sars-associated coronavirus replication in animal and human cell lines, Biochem. Biophys. Res. Commun. 326 (4) (2005) 905–908, https://doi.org/10.1016/j.bbrc.2004.11.128.

[18] G. Koren, S. King, S. Knowles, E. Phillips, Ribavirin in the treatment of sars: a new trick for an old drug? CMAJ (Can. Med. Assoc. J.) : Canadian Medical Association journal = journal de l'Association medicale canadienne 168 (10) (2003) 1289–1292. URL, https://pubmed.ncbi.nlm.nih.gov/12743076.

[19] J.A. Al-Tawfiq, H. Momattin, J. Dib, Z.A. Memish, Ribavirin and interferon therapy in patients infected with the middle east respiratory syndrome coronavirus: an observational study, Int. J. Infect. Dis. 20 (2014) 42–46, https://doi.org/10.1016/j.ijid.2013.12.003.

[20] Y. Wang, W. Li, Z. Jiang, X. Xi, Y. Zhu, Assessment of the efficacy and safety of ribavirin in treatment of coronavirus-related pneumonia (SARS, MERS and COVID-19), Medicine 99 (38) (2020), e22379, https://doi.org/10.1097/md.0000000000022379.

[21] Y.P. Chong, J.Y. Song, Y.B. Seo, J.-P. Choi, H.-S. Shin, Antiviral treatment guidelines for middle east respiratory syndrome, Infection & Chemotherapy 47 (3) (2015) 212, https://doi.org/10.3947/ic.2015.47.3.212.

[22] C.M. Booth, L.M. Matukas, G.A. Tomlinson, A.R. Rachlis, D.B. Rose, H.A. Dwosh, S.L. Walmsley, T. Mazzulli, M. Avendano, P. Derkach, I.E. Ephtimios, I. Kitai, B. D. Mederski, S.B. Shadowitz, W.L. Gold, L.A. Hawryluck, E. Rea, J.S. Chenkin, D. W. Cescon, S.M. Poutanen, A.S. Detsky, Clinical features and short-term outcomes of 144 patients with SARS in the greater toronto area, JAMA 289 (21) (2003) 2801–2809, https://doi.org/10.1001/jama.289.21.JOC30885.

[23] J.S. Khalili, H. Zhu, N.S.A. Mak, Y. Yan, Y. Zhu, Novel coronavirus treatment with ribavirin: groundwork for an evaluation concerning covid-19, J. Med. Virol. 92 (7) (2020) 740–746, https://doi.org/10.1002/jmv.25798.

[24] A. Boretti, Favipiravir use for sars cov-2 infection, Pharmacol. Rep. : PR 72 (6) (2020) 1542–1552, https://doi.org/10.1007/s43440-020-00175-2.

[25] S. Jomah, S.M.B. Asdaq, M.J. Al-Yamani, Clinical efficacy of antivirals against novel coronavirus (covid-19): a review, J. Infect.Public Health 13 (9) (2020) 1187–1195, https://doi.org/10.1016/j.jiph.2020.07.013, pMC7396961[pmcid].

[26] K. Doi, M. Ikeda, N. Hayase, K. Moriya, N. Morimura, H. Maehara, S. Tagami, K. Fukushima, N. Misawa, Y. Inoue, H. Nakamura, D. Takai, M. Kurimoto, K. Tokunaga, M. Yamamoto, I. Hirayama, R. Horie, Y. Endo, K. Hiwatashi, M. Shikama, D. Jubishi, Y. Kanno, K. Okamoto, S. Harada, S. Okugawa, K. Miyazono, Y. Seto, J.-i. Inoue, the COVID-UTH Study Group, Nafamostat mesylate treatment in combination with favipiravir for patients critically ill with covid-19: a case series, Crit. Care 24 (1) (2020) 392, https://doi.org/10.1186/s13054-020-03078-z.

[27] H. Takahashi, Y. Iwasaki, T. Watanabe, N. Ichinose, Y. Okada, A. Oiwa, T. Kobayashi, M. Moriya, T. Oda, Case studies of SARS-CoV-2 treated with favipiravir among patients in critical or severe condition, Int. J. Infect. Dis. 100 (2020) 283–285, https://doi.org/10.1016/j.ijid.2020.08.047.

[28] Q. Cai, M. Yang, D. Liu, J. Chen, D. Shu, J. Xia, X. Liao, Y. Gu, Q. Cai, Y. Yang, C. Shen, X. Li, L. Peng, D. Huang, J. Zhang, S. Zhang, F. Wang, J. Liu, L. Chen, S. Chen, Z. Wang, Z. Zhang, R. Cao, W. Zhong, Y. Liu, L. Liu, Experimental treatment with favipiravir for covid-19: an open-label control study, Engineering 6 (10) (2020) 1192–1198, https://doi.org/10.1016/j.eng.2020.03.007.

[29] U. Agrawal, R. Raju, Z.F. Udwadia, Favipiravir: a new and emerging antiviral option in covid-19, Med. J. Armed Forces India 76 (4) (2020) 370–376, https://doi.org/10.1016/j.mjafi.2020.08.004.

[30] T. P. Sheahan, A. C. Sims, R. L. Graham, V. D. Menachery, L. E. Gralinski, J. B. Case, S. R. Leist, K. Pyrc, J. Y. Feng, I. Trantcheva, R. Bannister, Y. Park, D. Babusis, M. O. Clarke, R. L. Mackman, J. E. Spahn, C. A. Palmiotti, D. Siegel, A. S. Ray, T. Cihlar, R. Jordan, M. R. Denison, R. S. Baric, Broad-spectrum antiviral gs-5734 inhibits both epidemic and zoonotic coronaviruses, Sci. Transl. Med. 9 (396). doi:10.1126/scitranslmed.aal3653..

[31] W. Yin, C. Mao, X. Luan, D.-D. Shen, Q. Shen, H. Su, X. Wang, F. Zhou, W. Zhao, M. Gao, S. Chang, Y.-C. Xie, G. Tian, H.-W. Jiang, S.-C. Tao, J. Shen, Y. Jiang, H. Jiang, Y. Xu, S. Zhang, Y. Zhang, H.E. Xu, Structural basis for inhibition of the rna-dependent rna polymerase from sars-cov-2 by remdesivir, Science 368 (6498) (2020) 1499–1504, https://doi.org/10.1126/science.abc1560.

[32] A.J. Brown, J.J. Won, R.L. Graham, K.H. Dinnon, A.C. Sims, J.Y. Feng, T. Cihlar, M.R. Denison, R.S. Baric, T.P. Sheahan, Broad spectrum antiviral remdesivir inhibits human endemic and zoonotic deltacoronaviruses with a highly divergent rna dependent rna polymerase, Antivir. Res. 169 (2019) 104541, https://doi.org/10.1016/j.antiviral.2019.104541.

[33] J.H. Beigel, K.M. Tomashek, L.E. Dodd, A.K. Mehta, B.S. Zingman, A.C. Kalil, E. Hohmann, H.Y. Chu, A. Luetkemeyer, S. Kline, D. Lopez de Castilla, R. W. Finberg, K. Dierberg, V. Tapson, L. Hsieh, T.F. Patterson, R. Paredes, D. A. Sweeney, W.R. Short, G. Touloumi, D.C. Lye, N. Ohmagari, M.-d. Oh, G. M. Ruiz-Palacios, T. Benfield, G. Fätkenheuer, M.G. Kortepeter, R.L. Atmar, C. B. Creech, J. Lundgren, A.G. Babiker, S. Pett, J.D. Neaton, T.H. Burgess, T. Bonnett, M. Green, M. Makowski, A. Osinusi, S. Nayak, H.C. Lane, Remdesivir for the treatment of covid-19 - final report, N. Engl. J. Med. 383 (19) (2020) 1813–1826, https://doi.org/10.1056/NEJMoa2007764.

[34] M.L. Holshue, C. DeBolt, S. Lindquist, K.H. Lofy, J. Wiesman, H. Bruce, C. Spitters, K. Ericson, S. Wilkerson, A. Tural, G. Diaz, A. Cohn, L. Fox, A. Patel, S. I. Gerber, L. Kim, S. Tong, X. Lu, S. Lindstrom, M.A. Pallansch, W.C. Weldon, H. M. Biggs, T.M. Uyeki, S.K. Pillai, First case of 2019 novel coronavirus in the United States, N. Engl. J. Med. 382 (10) (2020) 929–936, https://doi.org/10.1056/NEJMoa2001191, pMID: 32004427.

[35] A.J. Pruijssers, A.S. George, A. Schäfer, S.R. Leist, L.E. Gralinksi, K.H. Dinnon, B. L. Yount, M.L. Agostini, L.J. Stevens, J.D. Chappell, X. Lu, T.M. Hughes, K. Gully, D.R. Martinez, A.J. Brown, R.L. Graham, J.K. Perry, V. Du Pont, J. Pitts, B. Ma, D. Babusis, E. Murakami, J.Y. Feng, J.P. Bilello, D.P. Porter, T. Cihlar, R.S. Baric, M.R. Denison, T.P. Sheahan, Remdesivir inhibits sars-cov-2 in human lung cells and chimeric sars-cov expressing the sars-cov-2 rna polymerase in mice, Cell Rep. 32 (3) (2020) 107940, https://doi.org/10.1016/j.celrep.2020.107940.

[36] Y. Wang, D. Zhang, G. Du, R. Du, J. Zhao, Y. Jin, S. Fu, L. Gao, Z. Cheng, Q. Lu, Y. Hu, G. Luo, K. Wang, Y. Lu, H. Li, S. Wang, S. Ruan, C. Yang, C. Mei, Y. Wang, D. Ding, F. Wu, X. Tang, X. Ye, Y. Ye, B. Liu, J. Yang, W. Yin, A. Wang, G. Fan, F. Zhou, Z. Liu, X. Gu, J. Xu, L. Shang, Y. Zhang, L. Cao, T. Guo, Y. Wan, H. Qin, Y. Jiang, T. Jaki, F.G. Hayden, P.W. Horby, B. Cao, C. Wang, Remdesivir in adults with severe covid-19: a randomised, double-blind, placebo-controlled, multicentre trial, Lancet 395 (10236) (2020) 1569–1578, https://doi.org/10.1016/S0140-6736(20)31022-9.

[37] W.-C. Ko, J.-M. Rolain, N.-Y. Lee, P.-L. Chen, C.-T. Huang, P.-I. Lee, P.-R. Hsueh, Arguments in favour of remdesivir for treating sars-cov-2 infections, Int. J. Antimicrob. Agents 55 (4) (2020) 105933, https://doi.org/10.1016/j.ijantimicag.2020.105933.

[38] M. Martinot, A. Jary, S. Fafi-Kremer, V. Leducq, H. Delagreverie, M. Garnier, J. Pacanowski, A. Mékinian, F. Pirenne, P. Tiberghien, V. Calvez, C. Humbrecht, A.-G. Marcelin, K. Lacombe, Remdesivir failure with SARS-CoV-2 RNA-dependent RNA-polymerase mutation in a B-cell immunodeficient patient with protracted Covid-19, Clin. Infect. Dis.doi:10.1093/cid/ciaa1474..

[39] E.K. McCreary, D.C. Angus, Efficacy of remdesivir in COVID-19, JAMA 324 (11) (2020) 1041–1042, https://doi.org/10.1001/jama.2020.16337.

[40] E. Schrezenmeier, T. Dörner, Mechanisms of action of hydroxychloroquine and chloroquine: implications for rheumatology, Nat. Rev. Rheumatol. 16 (3) (2020) 155–166, https://doi.org/10.1038/s41584-020-0372-x.

[41] P. Gautret, J.-C. Lagier, P. Parola, V.T. Hoang, L. Meddeb, M. Mailhe, B. Doudier, J. Courjon, V. Giordanengo, V.E. Vieira, H.T. Dupont, S. Honoré, P. Colson, E. Chabrière, B.L. Scola, J.-M. Rolain, P. Brouqui, D. Raoult, Hydroxychloroquine and azithromycin as a treatment of COVID-19: results of an open-label non-randomized clinical trial, Int. J. Antimicrob. Agents 56 (1) (2020) 105949, https://doi.org/10.1016/j.ijantimicag.2020.105949.

[42] J. Chen, D. Liu, L. Liu, P. Liu, Q. Xu, L. Xia, Y. Ling, D. Huang, S. Song, D. Zhang, et al., A pilot study of hydroxychloroquine in treatment of patients with moderate covid-19, Zhejiang da xue xue bao. Yi xue ban = Journal of Zhejiang University. Medical sciences 49 (2)..

[43] B. Yu, C. Li, P. Chen, N. Zhou, L. Wang, J. Li, H. Jiang, D.-W. Wang, Low dose of hydroxychloroquine reduces fatality of critically ill patients with COVID-19, Sci. China Life Sci. 63 (10) (2020) 1515–1521, https://doi.org/10.1007/s11427-020-1732-2.

[44] J. M. Sanders, M. L. Monogue, T. Z. Jodlowski, J. B. Cutrell, Pharmacologic treatments for coronavirus disease 2019 (COVID-19), JAMAdoi:10.1001/jama.2020.6019.

[45] M. Mahévas, V.-T. Tran, M. Roumier, A. Chabrol, R. Paule, C. Guillaud, E. Fois, R. Lepeule, T.-A. Szwebel, F.-X. Lescure, F. Schlemmer, M. Matignon, M. Khellaf, E. Crickx, B. Terrier, C. Morbieu, P. Legendre, J. Dang, Y. Schoindre, J.-M. Pawlotsky, M. Michel, E. Perrodeau, N. Carlier, N. Roche, V. de Lastours, C. Ourghanlian, S. Kerneis, P. Ménager, L. Mouthon, E. Audureau, P. Ravaud, B. Godeau, S. Gallien, N. Costedoat-Chalumeau, Clinical efficacy of

hydroxychloroquine in patients with covid-19 pneumonia who require oxygen: observational comparative study using routine care data, BMJ (2020) m1844, https://doi.org/10.1136/bmj.m1844.
[46] M.G.S. Borba, F.F.A. Val, V.S. Sampaio, M.A.A. Alexandre, G.C. Melo, M. Brito, M. P.G. Mourão, J.D. Brito-Sousa, D.B. da Silva, M.V.F. Guerra, L.A. Hajjar, R. C. Pinto, A.A.S. Balieiro, A.G.F. Pacheco, J.D.O. Santos, F.G. Naveca, M.S. Xavier, A.M. Siqueira, A. Schwarzbold, J. Croda, M.L. Nogueira, G.A.S. Romero, Q. Bassat, C.J. Fontes, B.C. Albuquerque, C.-T. Daniel-Ribeiro, W.M. Monteiro, Marcus Vinícius Guimarães Lacerda, Effect of high vs low doses of chloroquine diphosphate as adjunctive therapy for patients hospitalized with severe acute respiratory syndrome coronavirus 2 (SARS-CoV-2) infection, JAMA Network Open 3 (4) (2020), e208857, https://doi.org/10.1001/jamanetworkopen.2020.8857.
[47] F. Bessière, H. Roccia, A. Delinière, R. Charrière, P. Chevalier, L. Argaud, M. Cour, Assessment of QT intervals in a case series of patients with coronavirus disease 2019 (COVID-19) infection treated with hydroxychloroquine alone or in combination with azithromycin in an intensive care unit, JAMA Cardiology 5 (9) (2020) 1067, https://doi.org/10.1001/jamacardio.2020.1787.
[48] M. Saleh, J. Gabriels, D. Chang, B.S. Kim, A. Mansoor, E. Mahmood, P. Makker, H. Ismail, B. Goldner, J. Willner, S. Beldner, R. Mitra, R. John, J. Chinitz, N. Skipitaris, S. Mountantonakis, L.M. Epstein, Effect of chloroquine, hydroxychloroquine, and azithromycin on the corrected qt interval in patients with sars-cov-2 infection, Circulation: Arrhythmia and Electrophysiology 13 (6) (2020), e008662, https://doi.org/10.1161/CIRCEP.120.008662.
[49] R.I. Rynes, H.N. Bernstein, Ophthalmologic safety profile of antimalarial drugs, Lupus 2 (1_suppl) (1993) 17–19, https://doi.org/10.1177/0961203393002001051.
[50] D.E. Gordon, G.M. Jang, M. Bouhaddou, J. Xu, K. Obernier, K.M. White, M. J. O'Meara, V.V. Rezelj, J.Z. Guo, D.L. Swaney, T.A. Tummino, R. Hüttenhain, R. M. Kaake, A.L. Richards, B. Tutuncuoglu, H. Foussard, J. Batra, K. Haas, M. Modak, M. Kim, P. Haas, B.J. Polacco, H. Braberg, J.M. Fabius, M. Eckhardt, M. Soucheray, M.J. Bennett, M. Cakir, M.J. McGregor, Q. Li, B. Meyer, F. Roesch, T. Vallet, A. Mac Kain, L. Miorin, E. Moreno, Z.Z.C. Naing, Y. Zhou, S. Peng, Y. Shi, Z. Zhang, W. Shen, I.T. Kirby, J.E. Melnyk, J.S. Chorba, K. Lou, S.A. Dai, I. Barrio-Hernandez, D. Memon, C. Hernandez-Armenta, J. Lyu, C.J.P. Mathy, T. Perica, K.B. Pilla, S.J. Ganesan, D.J. Saltzberg, R. Rakesh, X. Liu, S. B. Rosenthal, L. Calviello, S. Venkataramanan, J. Liboy-Lugo, Y. Lin, X.-P. Huang, Y. Liu, S.A. Wankowicz, M. Bohn, M. Safari, F.S. Ugur, C. Koh, N.S. Savar, Q. D. Tran, D. Shengjuler, S.J. Fletcher, M.C. O'Neal, Y. Cai, J.C.J. Chang, D. J. Broadhurst, S. Klippsten, P.P. Sharp, N.A. Wenzell, D. Kuzuoglu-Ozturk, H.-Y. Wang, R. Trenker, J.M. Young, D.A. Cavero, J. Hiatt, T.L. Roth, U. Rathore, A. Subramanian, J. Noack, M. Hubert, R.M. Stroud, A.D. Frankel, O.S. Rosenberg, K.A. Verba, D.A. Agard, M. Ott, M. Emerman, N. Jura, M. von Zastrow, E. Verdin, A. Ashworth, O. Schwartz, C. d'Enfert, S. Mukherjee, M. Jacobson, H.S. Malik, D. G. Fujimori, T. Ideker, C.S. Craik, S.N. Floor, J.S. Fraser, J.D. Gross, A. Sali, B. L. Roth, D. Ruggero, J. Taunton, T. Kortemme, P. Beltrao, M. Vignuzzi, A. García-Sastre, K.M. Shokat, B.K. Shoichet, N.J. Krogan, A sars-cov-2 protein interaction map reveals targets for drug repurposing, Nature 583 (7816) (2020) 459–468, https://doi.org/10.1038/s41586-020-2286-9.
[51] P. Krafcikova, J. Silhan, R. Nencka, E. Boura, Structural analysis of the sars-cov-2 methyltransferase complex involved in rna cap creation bound to sinefungin, Nat. Commun. 11 (1) (2020) 3717, https://doi.org/10.1038/s41467-020-17495-9.
[52] S. Xia, Y. Zhu, M. Liu, Q. Lan, W. Xu, Y. Wu, T. Ying, S. Liu, Z. Shi, S. Jiang, L. Lu, Fusion mechanism of 2019-ncov and fusion inhibitors targeting hr1 domain in spike protein, Cell. Mol. Immunol. 17 (7) (2020) 765–767, https://doi.org/10.1038/s41423-020-0374-2.
[53] J. Luan, Y. Lu, X. Jin, L. Zhang, Spike protein recognition of mammalian ace2 predicts the host range and an optimized ace2 for sars-cov-2 infection, Biochem. Biophys. Res. Commun. 526 (1) (2020) 165–169, https://doi.org/10.1016/j.bbrc.2020.03.047.
[54] J. Lan, J. Ge, J. Yu, S. Shan, H. Zhou, S. Fan, Q. Zhang, X. Shi, Q. Wang, L. Zhang, X. Wang, Structure of the SARS-CoV-2 spike receptor-binding domain bound to the ACE2 receptor, Nature 581 (7807) (2020) 215–220, https://doi.org/10.1038/s41586-020-2180-5.
[55] A.C. Walls, Y.J. Park, M.A. Tortorici, A. Wall, A.T. McGuire, D. Veesler, Structure, function, and antigenicity of the SARS-CoV-2 spike glycoprotein, Cell 181 (2) (2020) 281–292, https://doi.org/10.1016/j.cell.2020.02.058, e6.
[56] J.L. Daly, B. Simonetti, K. Klein, K.-E. Chen, M.K. Williamson, C. Antón-Plágaro, D.K. Shoemark, L. Simón-Gracia, M. Bauer, R. Hollandi, U.F. Greber, P. Horvath, R.B. Sessions, A. Helenius, J.A. Hiscox, T. Teesalu, D.A. Matthews, A.D. Davidson, B.M. Collins, P.J. Cullen, Y. Yamauchi, Neuropilin-1 is a host factor for sars-cov-2 infection, Science 370 (6518) (2020) 861–865, https://doi.org/10.1126/science.abd3072.
[57] L. Cantuti-Castelvetri, R. Ojha, L.D. Pedro, M. Djannatian, J. Franz, S. Kuivanen, F. van der Meer, K. Kallio, T. Kaya, M. Anastasina, T. Smura, L. Levanov, L. Szirovicza, A. Tobi, H. Kallio-Kokko, P. Österlund, M. Joensuu, F.A. Meunier, S. J. Butcher, M.S. Winkler, B. Mollenhauer, A. Helenius, O. Gokce, T. Teesalu, J. Hepojoki, O. Vapalahti, C. Stadelmann, G. Balistreri, M. Simons, Neuropilin-1 facilitates sars-cov-2 cell entry and infectivity, Science 370 (6518) (2020) 856–860, https://doi.org/10.1126/science.abd2985.
[58] M. Smith, J. Smith, Repurposing Therapeutics for Covid-19: Supercomputer-Based Docking to the Sars-Cov-2 Viral Spike Protein and Viral Spike Protein-Human Ace2 Interfacedoi:10.26434/chemrxiv.11871402.v3..
[59] C. Mu, Y. Sheng, Q. Wang, A. Amin, X. Li, Y. Xie, Potential compound from herbal food of rhizoma polygonati for treatment of covid-19 analyzed by network pharmacology: viral and cancer signaling mechanisms, J.Funct. Foods 77 (2021), https://doi.org/10.1016/j.jff.2020.104149, 104149–104149.
[60] S. Choudhary, Y.S. Malik, S. Tomar, Identification of sars-cov-2 cell entry inhibitors by drug repurposing using in silico structure-based virtual screening approach, Front. Immunol. 11 (2020) 1664, https://doi.org/10.3389/fimmu.2020.01664.
[61] S. Unni, S. Aouti, S. Thiyagarajan, B. Padmanabhan, Identification of a repurposed drug as an inhibitor of spike protein of human coronavirus sars-cov-2 by computational methods, J. Biosci. 45 (1) (2020) 1–20.
[62] M.R. Rameshkumar, P. Indu, N. Arunagirinathan, B. Venkatadri, H.A. El-Serehy, A. Ahmad, Computational selection of flavonoid compounds as inhibitors against sars-cov-2 main protease, rna-dependent rna polymerase and spike proteins: a molecular docking study, Saudi J. Biol. Sci. 28 (1) (2021) 448–458.
[63] Y. Yang, M.S. Islam, J. Wang, Y. Li, X. Chen, Traditional Chinese medicine in the treatment of patients infected with 2019-new coronavirus (sars-cov-2): a review and perspective, Int. J. Biol. Sci. 16 (10) (2020) 1708.
[64] D. hai Zhang, K. lun Wu, X. Zhang, S. qiong Deng, B. Peng, In silico screening of Chinese herbal medicines with the potential to directly inhibit 2019 novel coronavirus, J. Integr. Med. 18 (2) (2020) 152–158, https://doi.org/10.1016/j.joim.2020.02.005.
[65] S.K. Sinha, A. Shakya, S.K. Prasad, S. Singh, N.S. Gurav, R.S. Prasad, S.S. Gurav, An in-silico evaluation of different saikosaponins for their potency against sars-cov-2 using nsp15 and fusion spike glycoprotein as targets, J. Biomol. Struct. Dyn. 39 (9) (2021) 3244–3255, https://doi.org/10.1080/07391102.2020.1762741, pMID: 32345124.
[66] C. Mu, Y. Sheng, Q. Wang, A. Amin, X. Li, Y. Xie, Potential compound from herbal food of rhizoma polygonati for treatment of covid-19 analyzed by network pharmacology: viral and cancer signaling mechanisms, Journal of Functional Foods 77 (2021) 104149, https://doi.org/10.1016/j.jff.2020.104149.
[67] S.K. Sinha, S.K. Prasad, M.A. Islam, S.S. Gurav, R.B. Patil, N.A. AlFaris, T. S. Aldayel, N.M. AlKehayez, S.M. Wabaidur, A. Shakya, Identification of bioactive compounds from glycyrrhiza glabra as possible inhibitor of sars-cov-2 spike glycoprotein and non-structural protein-15: a pharmacoinformatics study, 0 (0), J. Biomol. Struct. Dyn. (2020) 1–15, https://doi.org/10.1080/07391102.2020.1779132. pMID: 32345124.
[68] S. Yu, Y. Zhu, J. Xu, G. Yao, P. Zhang, M. Wang, Y. Zhao, G. Lin, H. Chen, L. Chen, J. Zhang, Glycyrrhizic acid exerts inhibitory activity against the spike protein of sars-cov-2, Phytomedicine 85 (2021) 153364, https://doi.org/10.1016/j.phymed.2020.153364.
[69] M. Ye, G. Luo, D. Ye, M. She, N. Sun, Y.-J. Lu, J. Zheng, Network pharmacology, molecular docking integrated surface plasmon resonance technology reveals the mechanism of toujie quwen granules against coronavirus disease 2019 pneumonia, Phytomedicine 85 (2021) 153401, https://doi.org/10.1016/j.phymed.2020.153401.
[70] J. Zhou, G. Xie, X. Yan, Encyclopedia of Traditional Chinese Medicines - Molecular Structures, Pharmacological Activities, Natural Sources and Applications, Springer Berlin Heidelberg, 2011, https://doi.org/10.1007/978-3-642-16744-7.
[71] Schrödinger Release 2020-4: LigPrep, Schrödinger, LLC, New York, NY.
[72] R.V. Chikhale, S.S. Gurav, R.B. Patil, S.K. Sinha, S.K. Prasad, A. Shakya, S. K. Shrivastava, N.S. Gurav, R.S. Prasad, Sars-cov-2 host entry and replication inhibitors from indian ginseng: an in-silico approach, 0 (0), J. Biomol. Struct. Dyn. (2020) 1–12, https://doi.org/10.1080/07391102.2020.1778539. pMID: 32568012.
[73] D.C. Hall, H.-F. Ji, A search for medications to treat covid-19 via in silico molecular docking models of the sars-cov-2 spike glycoprotein and 3cl protease, Trav. Med. Infect. Dis. 35 (2020) 101646, https://doi.org/10.1016/j.tmaid.2020.101646.
[74] E. Harder, W. Damm, J. Maple, C. Wu, M. Reboul, J.Y. Xiang, L. Wang, D. Lupyan, M.K. Dahlgren, J.L. Knight, J.W. Kaus, D.S. Cerutti, G. Krilov, W.L. Jorgensen, R. Abel, R.A. Friesner, OPLS3: a force field providing broad coverage of drug-like small molecules and proteins, J. Chem. Theor. Comput. 12 (1) (2015) 281–296, https://doi.org/10.1021/acs.jctc.5b00864.
[75] J.R. Greenwood, D. Calkins, A.P. Sullivan, J.C. Shelley, Towards the comprehensive, rapid, and accurate prediction of the favorable tautomeric states of drug-like molecules in aqueous solution, J. Comput. Aided Mol. Des. 24 (6–7) (2010) 591–604, https://doi.org/10.1007/s10822-010-9349-1.
[76] J.C. Shelley, A. Cholleti, L.L. Frye, J.R. Greenwood, M.R. Timlin, M. Uchimaya, Epik: a software program for pK a prediction and protonation state generation for drug-like molecules, J. Comput. Aided Mol. Des. 21 (12) (2007) 681–691, https://doi.org/10.1007/s10822-007-9133-z.
[77] Schrödinger Release 2021-1, Epik, Schrödinger, LLC, New York, NY, 2021.
[78] Schrödinger Release 2020-4: QikProp, Schrödinger, LLC, New York, NY.
[79] X. Huang, R. Pearce, Y. Zhang, De novo design of protein peptides to block association of the sars-cov-2 spike protein with human ace2, Aging 12 (12) (2020) 11263–11276, pMC7343451[pmcid]. URL, https://pubmed.ncbi.nlm.nih.gov/32544884.
[80] Schrödinger Release 2020–1: Protein Preparation Wizard, Epik, Schrödinger, LLC, New York, NY, 2020. Impact, Schrödinger, LLC, New York, NY, 2020; Prime, Schrödinger, LLC, New York, NY.
[81] M.P. Jacobson, R.A. Friesner, Z. Xiang, B. Honig, On the role of the crystal environment in determining protein side-chain conformations, J. Mol. Biol. 320 (3) (2002) 597–608, https://doi.org/10.1016/s0022-2836(02)00470-9.
[82] M.P. Jacobson, D.L. Pincus, C.S. Rapp, T.J. Day, B. Honig, D.E. Shaw, R. A. Friesner, A hierarchical approach to all-atom protein loop prediction, Proteins:

Structure, Function, and Bioinformatics 55 (2) (2004) 351–367, https://doi.org/10.1002/prot.10613.
[83] Schrödinger Release 2021-1: Prime, Schrödinger, LLC, New York, NY, 2021.
[84] G.M. Sastry, M. Adzhigirey, T. Day, R. Annabhimoju, W. Sherman, Protein and ligand preparation: parameters, protocols, and influence on virtual screening enrichments, J. Comput. Aided Mol. Des. 27 (3) (2013) 221–234, https://doi.org/10.1007/s10822-013-9644-8.
[85] R.A. Friesner, J.L. Banks, R.B. Murphy, T.A. Halgren, J.J. Klicic, D.T. Mainz, M. P. Repasky, E.H. Knoll, M. Shelley, J.K. Perry, D.E. Shaw, P. Francis, P.S. Shenkin, Glide: a new approach for rapid, accurate docking and scoring. 1. method and assessment of docking accuracy, J. Med. Chem. 47 (7) (2004) 1739–1749, https://doi.org/10.1021/jm0306430.
[86] T.A. Halgren, R.B. Murphy, R.A. Friesner, H.S. Beard, L.L. Frye, W.T. Pollard, J. L. Banks, Glide: a new approach for rapid, accurate docking and scoring. 2. enrichment factors in database screening, J. Med. Chem. 47 (7) (2004) 1750–1759, https://doi.org/10.1021/jm030644s.
[87] R.A. Friesner, R.B. Murphy, M.P. Repasky, L.L. Frye, J.R. Greenwood, T. A. Halgren, P.C. Sanschagrin, D.T. Mainz, Extra precision glide:docking and scoring incorporating a model of hydrophobic enclosure for protein-ligand complexes, J. Med. Chem. 49 (21) (2006) 6177–6196, https://doi.org/10.1021/jm051256o.
[88] Schrödinger Release 2021-1: Glide, Schrödinger, LLC, New York, NY, 2021.
[89] C. Sachdeva, A. Wadhwa, A. Kumari, F. Hussain, P. Jha, N.K. Kaushik, In silico potential of approved antimalarial drugs for repurposing against covid-19, OMICS 24 (10) (2020) 568–580, https://doi.org/10.1089/omi.2020.0071, pMID: 32757981.
[90] H.J.C. Berendsen, J.P.M. Postma, W.F. van Gunsteren, J. Hermans, Interaction models for water in relation to protein hydration, in: The Jerusalem Symposia on Quantum Chemistry and Biochemistry, Springer Netherlands, 1981, pp. 331–342, https://doi.org/10.1007/978-94-015-7658-1_21.
[91] H.J.C. Berendsen, J.R. Grigera, T.P. Straatsma, The missing term in effective pair potentials, J. Phys. Chem. 91 (24) (1987) 6269–6271, https://doi.org/10.1021/j100308a038.
[92] K. Takemura, A. Kitao, Water model tuning for improved reproduction of rotational diffusion and NMR spectral density, J. Phys. Chem. B 116 (22) (2012) 6279–6287, https://doi.org/10.1021/jp301100g.
[93] K.J. Bowers, D.E. Chow, H. Xu, R.O. Dror, M.P. Eastwood, B.A. Gregersen, J. L. Klepeis, I. Kolossvary, M.A. Moraes, F.D. Sacerdoti, J.K. Salmon, Y. Shan, D. E. Shaw, Scalable algorithms for molecular dynamics simulations on commodity clusters, in: ACM/IEEE SC 2006 Conference (SC06), IEEE, 2006, https://doi.org/10.1109/sc.2006.54.
[94] Schrödinger Release 2020-4: Desmond Molecular Dynamics System, D. E. Shaw Research, New York, NY, 2020. Maestro-Desmond Interoperability Tools, Schrödinger, New York, NY.
[95] V. Krautler, W.F. van Gunsteren, P.H. Hünenberger, A fast SHAKE algorithm to solve distance constraint equations for small molecules in molecular dynamics simulations, J. Comput. Chem. 22 (5) (2001) 501–508, https://doi.org/10.1002/1096-987x(20010415)22:5<501::aid-jcc1021>3.0.co;2-v.
[96] D.J. Evans, B.L. Holian, The nose–hoover thermostat, J. Chem. Phys. 83 (8) (1985) 4069–4074, https://doi.org/10.1063/1.449071.
[97] Y. Shan, J.L. Klepeis, M.P. Eastwood, R.O. Dror, D.E. Shaw, Gaussian split ewald: a fast ewald mesh method for molecular simulation, J. Chem. Phys. 122 (5) (2005), 054101, https://doi.org/10.1063/1.1839571.
[98] H.J.C. Berendsen, J.P.M. Postma, W.F. van Gunsteren, A. DiNola, J.R. Haak, Molecular dynamics with coupling to an external bath, J. Chem. Phys. 81 (8) (1984) 3684–3690, https://doi.org/10.1063/1.448118.
[99] The PyMOL Molecular Graphics System, Version 1.8 Schrödinger LLC.
[100] D. Chen, N. Oezguen, P. Urvil, C. Ferguson, S.M. Dann, T.C. Savidge, Regulation of protein-ligand binding affinity by hydrogen bond pairing, Science Advances 2 (3) (2016), e1501240, https://doi.org/10.1126/sciadv.1501240.
[101] W. Wu, R. Li, X. Li, J. He, S. Jiang, S. Liu, J. Yang, Quercetin as an antiviral agent inhibits influenza a virus (IAV) entry, Viruses 8 (1) (2015) 6, https://doi.org/10.3390/v8010006.
[102] P. Mehrbod, D. Hudy, D. Shyntum, J. Markowski, M.J. Łos, S. Ghavami, Quercetin as a natural therapeutic candidate for the treatment of influenza virus, Biomolecules 11 (1) (2020) 10, https://doi.org/10.3390/biom11010010.
[103] E. Fanunza, M. Iampietro, S. Distinto, A. Corona, M. Quartu, E. Maccioni, B. Horvat, E. Tramontano, Quercetin blocks ebola virus infection by counteracting the VP24 interferon-inhibitory function, Antimicrob. Agents Chemother. 64 (7). doi:10.1128/aac.00530-20..
[104] Nair, The flavonoid, quercetin, inhibits HIV-1 infection in normal peripheral blood mononuclear cells, Am. J. Infect. Dis. 5 (2) (2009) 135–141, https://doi.org/10.3844/ajidsp.2009.135.141.
[105] S. Jo, H. Kim, S. Kim, D.H. Shin, M.-S. Kim, Characteristics of flavonoids as potent MERS-CoV 3c-like protease inhibitors, Chem. Biol. Drug Des. 94 (6) (2019) 2023–2030, https://doi.org/10.1111/cbdd.13604.
[106] Y.B. Ryu, H.J. Jeong, J.H. Kim, Y.M. Kim, J.-Y. Park, D. Kim, T.T.H. Naguyen, S.-J. Park, J.S. Chang, K.H. Park, Biflavonoids from torreya nucifera displaying SARS-CoV 3clpro inhibition, Bioorg. Med. Chem. 18 (22) (2010) 7940–7947, https://doi.org/10.1016/j.bmc.2010.09.035.
[107] T.T.H. Nguyen, H.-J. Woo, H.-K. Kang, V.D. Nguyen, Y.-M. Kim, D.-W. Kim, S.-A. Ahn, Y. Xia, D. Kim, Flavonoid-mediated inhibition of SARS coronavirus 3c-like protease expressed in pichia pastoris, Biotechnol. Lett. 34 (5) (2012) 831–838, https://doi.org/10.1007/s10529-011-0845-8.
[108] O. Abian, D. Ortega-Alarcon, A. Jimenez-Alesanco, L. Ceballos-Laita, S. Vega, H. T. Reyburn, B. Rizzuti, A. Velazquez-Campoy, Structural stability of SARS-CoV-2 3clpro and identification of quercetin as an inhibitor by experimental screening, Int. J. Biol. Macromol. 164 (2020) 1693–1703, https://doi.org/10.1016/j.ijbiomac.2020.07.235.
[109] F. Huang, Y. Li, E.L.-H. Leung, X. Liu, K. Liu, Q. Wang, Y. Lan, X. Li, H. Yu, L. Cui, H. Luo, L. Luo, A review of therapeutic agents and Chinese herbal medicines against SARS-COV-2 (COVID-19), Pharmacol. Res. 158 (2020) 104929, https://doi.org/10.1016/j.phrs.2020.104929.
[110] M. Aucoin, K. Cooley, P.R. Saunders, V. Cardozo, D. Remy, H. Cramer, C.N. Abad, N. Hannan, The effect of quercetin on the prevention or treatment of COVID-19 and other respiratory tract infections in humans: a rapid review, Advances in Integrative Medicine 7 (4) (2020) 247–251, https://doi.org/10.1016/j.aimed.2020.07.007.
[111] A. Riva, M. Ronchi, G. Petrangolini, S. Bosisio, P. Allegrini, Improved oral absorption of quercetin from quercetin phytosome®, a new delivery system based on food grade lecithin, Eur. J. Drug Metab. Pharmacokinet. 44 (2) (2018) 169–177, https://doi.org/10.1007/s13318-018-0517-3.
[112] G. Williamson, A. Kerimi, Testing of natural products in clinical trials targeting the SARS-CoV-2 (covid-19) viral spike protein-angiotensin converting enzyme-2 (ACE2) interaction, Biochem. Pharmacol. 178 (2020) 114123, https://doi.org/10.1016/j.bcp.2020.114123.
[113] F. Di Pierro, A. Khan, A. Bertuccioli, P. Maffioli, G. Derosa, S. Khan, B. A. Khan, R. Nigar, I. Ujjan, B. R. Devraian, Quercetin phytosome® as a potential drug for covid-19, Minerva Gastroenterol. Dietol.:10.23736/S1121-421X.20.02771-3.